Neuron

Report

Translation of GGC repeat expansions into a toxic polyglycine protein in NIID defines a novel class of human genetic disorders: The polyG diseases

Graphical abstract

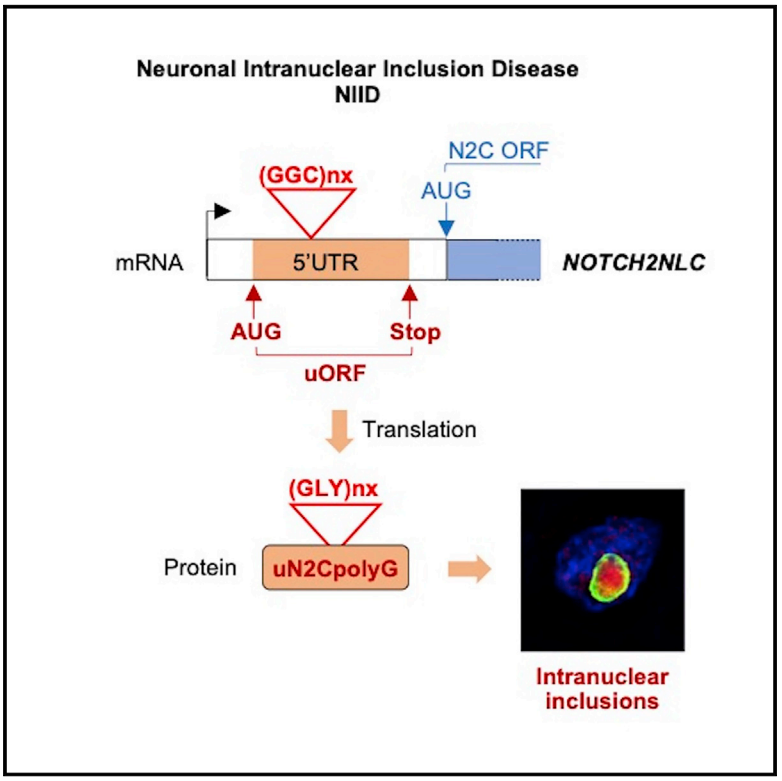

Highlights

- NIID is a neurodegenerative disease caused by expansion of GGC repeats in NOTCH2NLC
- These GGC repeats are translated into a polyglycine (polyG) protein
- The polyG protein is toxic and forms intranuclear inclusions in cells and animals
- Similarities between FXTAS and NIID define a new set of disorders: polyG diseases

Authors

Manon Boivin, Jianwen Deng, Véronique Pfister, ..., Jun Sone, Zhaoxia Wang, Nicolas Charlet-Berguerand

Correspondence

ncharlet@igbmc.fr

In brief

The neurodegenerative disease NIID is caused by an expansion of GGC repeats in NOTCH2NLC. Boivin et al. found that these repeats are translated into a toxic polyglycine (polyG) protein that forms intranuclear inclusions. An identical mechanism exists in FXTAS, unveiling a novel group of genetic pathologies, the polyG diseases.

Boivin et al., 2021, Neuron *109*, 1825–1835
June 2, 2021
https://doi.org/10.1016/j.neuron.2021.03.038

CellPress

Neuron

CellPress
OPEN ACCESS

Report

Translation of GGC repeat expansions into a toxic polyglycine protein in NIID defines a novel class of human genetic disorders: The polyG diseases

Manon Boivin,[1] Jianwen Deng,[2] Véronique Pfister,[1] Erwan Grandgirard,[1] Mustapha Oulad-Abdelghani,[1] Bastien Morlet,[1] Frank Ruffenach,[1] Luc Negroni,[1] Pascale Koebel,[1] Hugues Jacob,[1] Fabrice Riet,[1] Anke A. Dijkstra,[3] Kathryn McFadden,[4] Wiley A. Clayton,[5] Daojun Hong,[6] Hiroaki Miyahara,[7] Yasushi Iwasaki,[7] Jun Sone,[7,8] Zhaoxia Wang,[2] and Nicolas Charlet-Berguerand[1,9,*]

[1]Institut de Génétique et de Biologie Moléculaire et Cellulaire (IGBMC), INSERM U 1258, CNRS UMR 7104, University of Strasbourg, 67404 Illkirch, France
[2]Department of Neurology, Peking University First Hospital, Beijing 100034, China
[3]Department of Pathology, Amsterdam University Medical Centre, Amsterdam Neuroscience, VUmc, Amsterdam, the Netherlands
[4]Department of Pathology, IWK Health Centre, Halifax, NS B3K 6R8, Canada
[5]Department of Pathology, University of Pittsburgh Medical Center, Pittsburgh, PA 15213, USA
[6]Department of Neurology, First Affiliated Hospital of Nanchang University, Nanchang, China
[7]Department of Neuropathology, Institute for Medical Science of Aging, Aichi Medical University, Nagakute, Japan
[8]Department of Neurology, Suzuka National Hospital, Suzuka 513-8501, Japan
[9]Lead contact
*Correspondence: ncharlet@igbmc.fr
https://doi.org/10.1016/j.neuron.2021.03.038

SUMMARY

Neuronal intranuclear inclusion disease (NIID) is a neurodegenerative disease characterized by the presence of intranuclear inclusions of unknown origin. NIID is caused by an expansion of GGC repeats in the 5′ UTR of the NOTCH2NLC (N2C) gene. We found that these repeats are embedded in a small upstream open reading frame (uORF) (uN2C), resulting in their translation into a polyglycine-containing protein, uN2CpolyG. This protein accumulates in intranuclear inclusions in cell and mouse models and in tissue samples of individuals with NIID. Furthermore, expression of uN2CpolyG in mice leads to locomotor alterations, neuronal cell loss, and premature death of the animals. These results suggest that translation of expanded GGC repeats into a novel and pathogenic polyglycine-containing protein underlies the presence of intranuclear inclusions and neurodegeneration in NIID.

INTRODUCTION

More than 40 inherited human diseases are caused by expansion of microsatellites, short DNA tandem repeats variable in size and sequences. These microsatellite expansions are pathogenic by three main non-exclusive mechanisms (Nelson et al., 2013; Gao and Richter, 2017; Rodriguez and Todd, 2019). First, they can promote DNA epigenetic changes that inhibit transcription, resulting in loss of function of the allele carrying the repeats. Second, RNA transcripts containing the expanded repeats can bind to specific RNA binding proteins, potentially altering their localization and function. Third, expanded repeats can be translated by canonical initiation to AUG or near-cognate start codons or by translation initiation directly within the repeat through a novel mechanism called repeat-associated non-AUG (RAN) translation (Zu et al., 2011), into proteins containing a pathogenic stretch of repeated amino acids. Progress in long-read and whole-genome sequencing has recently unveiled a dozen novel microsatellite expansions located in the "non-coding" part of the human genome as pathogenic causes, notably an intronic AG-rich repeat expansion in the *RFC1* gene in cerebellar ataxia with neuropathy and bilateral vestibular areflexia syndrome (CANVAS) (Cortese et al., 2019; Rafehi et al., 2019); 6 similar intronic AT-rich repeat expansions in benign adult familial myoclonic epilepsy (BAFME) 1–6 and 5 similar 5′ UTR-embedded GC-rich repeat expansions in fragile X-associated tremor/ataxia syndrome (FXTAS), neuronal intranuclear inclusion disease (NIID), oculopharyngodistal myopathy (OPDM), and oculopharyngeal myopathy with leukoencephalopathy (OPML), neuromuscular and neurodegenerative syndromes with some overlapping symptoms and similar histopathological features (Hagerman et al., 2001; Ishiura et al., 2019; Sone et al., 2019; Deng et al., 2019, 2020; Tian et al., 2019; Xi et al., 2021; review in Ishiura and Tsuji, 2020).

Among these later disorders, NIID, also known as neuronal intranuclear hyaline inclusion disease (NIHID) and intranuclear

inclusion body disease (INIBD), is a rare genetic disease characterized by the presence of intranuclear inclusions in the central and peripheral nervous systems and in multiple other organs (Lindenberg et al., 1968; Munoz-Garcia and Ludwin, 1986; Sone et al., 2016). NIID age of onset is variable, and three subgroups (infant, juvenile, and adult) have been defined (Takahashi-Fujigasaki, 2003). Clinically, NIID is also tentatively divided in three subgroups: dementia dominant, parkinsonism dominant, and muscle weakness dominant. However, NIID symptoms are highly heterogenous, and overlap between subgroups is observed frequently, with variable muscle weakness associated with various dysfunctions of the central and peripheral nervous systems, which can include progressive dementia and cognitive impairment, parkinsonism, cerebellar ataxia, sensory disturbance, autonomic dysfunction, and/or peripheral neuropathy (Takahashi-Fujigasaki, 2003; Sone et al., 2016; Takahashi-Fujigasaki et al., 2016). Moreover, individuals with NIID with atypical presentation, such as essential tremors, multiple-systems atrophy, and amyotrophic lateral sclerosis, and various acute symptoms, including stroke-like episodes, epileptic seizures, and/or encephalitic episodes, have also been reported (Sone et al., 2016; Fang et al., 2020; Li et al., 2020; Sun et al., 2020; Yuan et al., 2020). As a consequence of these diverse ages of onset and clinical presentations, NIID diagnosis is most often confirmed by the widespread presence of characteristic eosinophilic intranuclear inclusions in neurons and glial cells in the central and peripheral nervous systems and in various other tissues (Chen et al., 2020a; Liu et al., 2008; Sone et al., 2005, 2011, 2014). These intranuclear inclusions are immunoreactive for various markers of the proteasomal and autophagic degradation pathways, including ubiquitin, sumo, and p62 (Pountney et al., 2003; Mori et al., 2012; Nakamura et al., 2014; Sone et al., 2016). Importantly, an expansion of GGC repeats located in the 5′ UTR of the NOTCH2NLC (Notch 2 N-terminal like C, N2C) gene has been found recently to be associated with individuals with familial and sporadic NIID, mostly in people of Asian origin (Sone et al., 2019; Ishiura et al., 2019; Deng et al., 2019; Tian et al., 2019). The NOTCH2NLA, NOTCH2NLB, and NOTCH2NLC genes are human-specific paralogs of *NOTCH2* exons 1–5, which encode Notch 2 N-terminal like (N2L) proteins that regulate Notch signaling to expand human neuronal progenitors during brain development (Fiddes et al., 2018; Suzuki et al., 2018). Alteration of NOTCH2NLC (N2C) protein function in NIID is unlikely because GGC repeats are located more than 100 nt upstream of the ATG start codon initiating the N2C open reading frame (ORF). Furthermore, NOTCH2NLC mRNA levels are unaltered in individuals with NIID (Sone et al., 2019; Ishiura et al., 2019; Tian et al., 2019). Thus, it remains to be determined how expansion of GGC repeats embedded in a predicted non-coding genomic region can lead to formation of intranuclear inclusions and cause neuronal cell death.

Here we find that the NOTCH2NLC GGC repeats are embedded in a small upstream open reading frame (uORF) located ahead of the main N2C ORF and encodes a small protein, uN2C. Of clinical importance is that GGC repeats embedded into the uN2C ORF are translated into a polyglycine stretch, resulting in expression of a uN2C polyglycine-containing protein (uN2CpolyG) in NIID. Antibodies developed against uN2CpolyG revealed its presence in the typical intranuclear inclusions in skin and brain sections of individuals with NIID. Furthermore, expression of uN2CpolyG in cell and animal models drives formation of p62-positive inclusions. Finally, expression of uN2CpolyG in mice is toxic, resulting in locomotor alterations, neuronal cell loss, and a reduced lifespan. These results are reminiscent of FXTAS, where an expansion of GGC repeats is embedded in a small upstream ORF, resulting in expression of a polyglycine-containing protein that, like uN2CpolyG, forms intranuclear inclusions and is toxic in cell and animal models (Hukema et al., 2015; Sellier et al., 2017; Todd et al., 2013). These data suggest the existence of a novel class of human genetic diseases where expanded GCC repeats are translated into pathogenic polyglycine (polyG) proteins.

RESULTS

NOTCH2NLC GGC repeats are translated into a polyG-containing protein

Because translation of expanded repeats into pathogenic stretches of repeated amino acids is an established mechanism of pathogenicity in microsatellite diseases, we investigated the potential translation of GGC repeats in NIID. First we cloned GGC repeats embedded in the human NOTCH2NLC exon 1 sequence and fused these repeats to GFP in the three possible frames (Figures 1A and S1A). These frames were called polyG, polyalanine (polyA), and polyarginine (polyR), according to the stretch of amino acids potentially encoded by the repeats. Cell transfection followed by immunoblotting against GFP or observation of GFP fluorescence indicated that NOTCH2NLC GGC repeats were translated predominantly in the glycine frame (Figures 1B and 1C). qRT-PCR quantification indicated that GGC repeats cloned in the three frames are similarly transcribed (Figure S1B). Furthermore, cell transfection of expanded GGC repeats cloned downstream of an artificial ATG start codon in the alanine or arginine frames and fused to GFP results in expression of ATG-driven polyA and polyR GFP-tagged proteins (Figures S1C and S1D). These controls indicate that the limited expression of polyA or polyR from the NOTCH2NLC 5′ UTR cannot be accounted for by lack of their expression at the RNA level or a technical bias impairing their detection and that the NOTCH2NLC GGC repeats are mainly translated into a polyG-containing protein, which was called uN2CpolyG (upstream of N2C polyG-containing protein).

To better characterize this protein, GGC repeats embedded in human NOTCH2NLC exon 1 and fused to GFP in the glycine frame were expressed in HEK293 cells, GFP immunoprecipitated, trypsin digested, and analyzed by mass spectrometry. Liquid chromatography-tandem mass spectrometry (LC-MS/MS) analysis confirmed that NOTCH2NLC GGC repeats are translated into a glycine stretch (Figures 1D and S1E). As a further control, treatment with lysostaphin, a glycylglycine endopeptidase, eliminated the N-terminal glycine stretch of uN2CpolyG-GFP, confirming its polyG nature (Figure 1E). Importantly, MS also revealed that GGC repeats are translated through initiation to a canonical AUG start codon located 15 nt before the repeats (Figures 1D and S1E). Deletion of this ATG codon abolished uN2CpolyG expression (Figure 1F). These data suggest

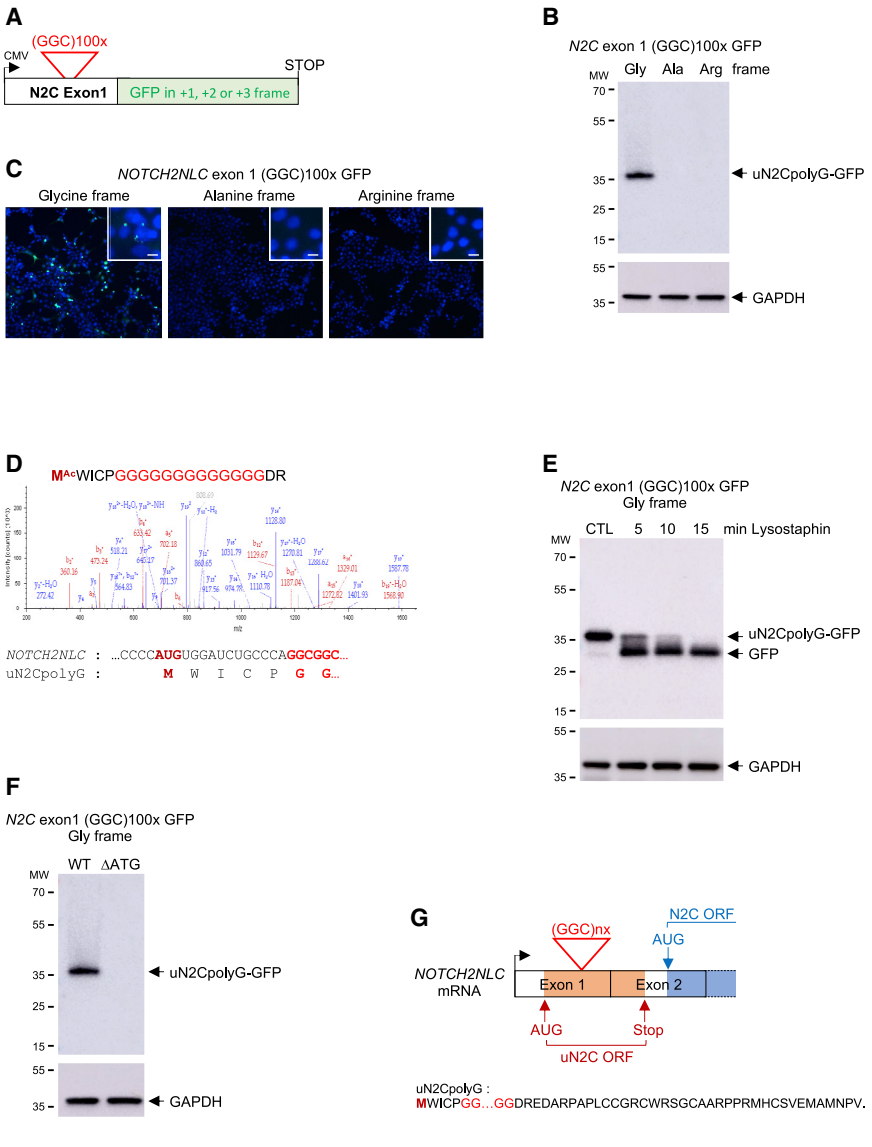

Figure 1. *NOTCH2NLC* GGC repeats are translated in a polyG-containing protein

(A) Schematic of NOTCH2NLC exon 1 with GGC repeats fused to GFP in the glycine, alanine, or arginine frame.

(B and C) Immunoblot against GFP (B) or direct fluorescence (C) of HEK293 cells transfected for 24 h with GGC repeats embedded in NOTCH2NLC exon 1 and fused to GFP in the three possible frames.

(D) Top panel: N-terminal sequence and corresponding LC-MS/MS spectra of GFP-immunoprecipitated and trypsin-digested protein expressed from uN2C-GFP-transfected HEK293 cells. Bottom panel: nucleotide and amino acid sequences corresponding to the NOTCH2NLC upstream ORF (uN2C) N terminus.

(E) Immunoblot against GFP or the glyceraldehyde 3-phosphate dehydrogenase (GAPDH) of lysostaphin-digested proteins extracted from uN2CpolyG-GFP-transfected HEK293 cells.

(F) Immunoblot against GFP or the GAPDH of proteins extracted from wild-type or mutant (ΔATG) uN2CpolyG-GFP-transfected HEK293 cells.

(G) Top panel: schematic of NOTCH2NLC exons 1 and 2. Bottom panel: amino acid sequence of the NOTCH2NLC upstream ORF (uN2C).

See also Figure S1.

that the NOTCH2NLC 5′ UTR contains a small upstream ORF, uN2C, that spans exons 1 and 2 and ends 8 nt before the ATG start site of the main NOTCH2NLC (N2C) ORF (Figures 1G and S1F). Consequently, the uN2CpolyG protein is composed of a short 5-amino-acid N terminus, a variable central glycine stretch corresponding to the number of GGC repeats, and a 38-amino-acid C-terminal part (Figure 1G).

The uN2polyG protein is present in NIID intranuclear inclusions

To confirm that NOTCH2NLC GGC repeats are translated into a polyG-containing protein in NIID, we developed two antibodies (4D12 and 4C4) directed against the uN2C C terminus, whose amino acid sequence differs from NOTCH2 and NOTCH2NLA predicted upstream ORFs (Figures 2A and S2A). Antibody specificity was confirmed by immunoblot and immunofluorescence (Figures S2B–S2D). Importantly, immunofluorescence using these antibodies revealed the presence of uN2CpolyG in the characteristic p62- and ubiquitin-positive intranuclear inclusions in skin and brain sections of individuals with NIID, carriers of an expansion of GGC repeats in NOTCH2NLC (N2C-NIID), but no staining in control age-matched individuals (Figures 2B–2E and S2E). As a control for uN2CpolyG staining specificity, identical results were observed with 4C4 and 4D12 antibodies, which are directed against different epitopes of the uN2C protein. Moreover, neither 4D12 nor 4C4 antibodies labeled p62-positive intranuclear inclusions of FMRpolyG in brain sections of FXTAS, a neurodegenerative disease caused, like NIID, by expanded GGC repeats translated into a polyG-containing protein (Figure S2F). Finally, quantification indicated quasi-complete co-localization of uN2CpolyG with p62-positive intranuclear inclusions in NIID (Figure S2G). These results demonstrate that NOTCH2NLC GGC repeat expansions are translated into a novel polyG-containing protein that is found in the typical intranuclear inclusions in individuals with N2C NIID.

During this analysis, we noted that various European individuals with NIID with typical p62-positive intranuclear inclusions were nevertheless negative for uN2CpolyG staining (Figure S2H; data are summarized in Table S1). Genetic analyses revealed that these individuals are negative for the NOTCH2NLC GGC expansion, which is consistent with a recent report showing that most Europeans with NIID are negative for this mutation

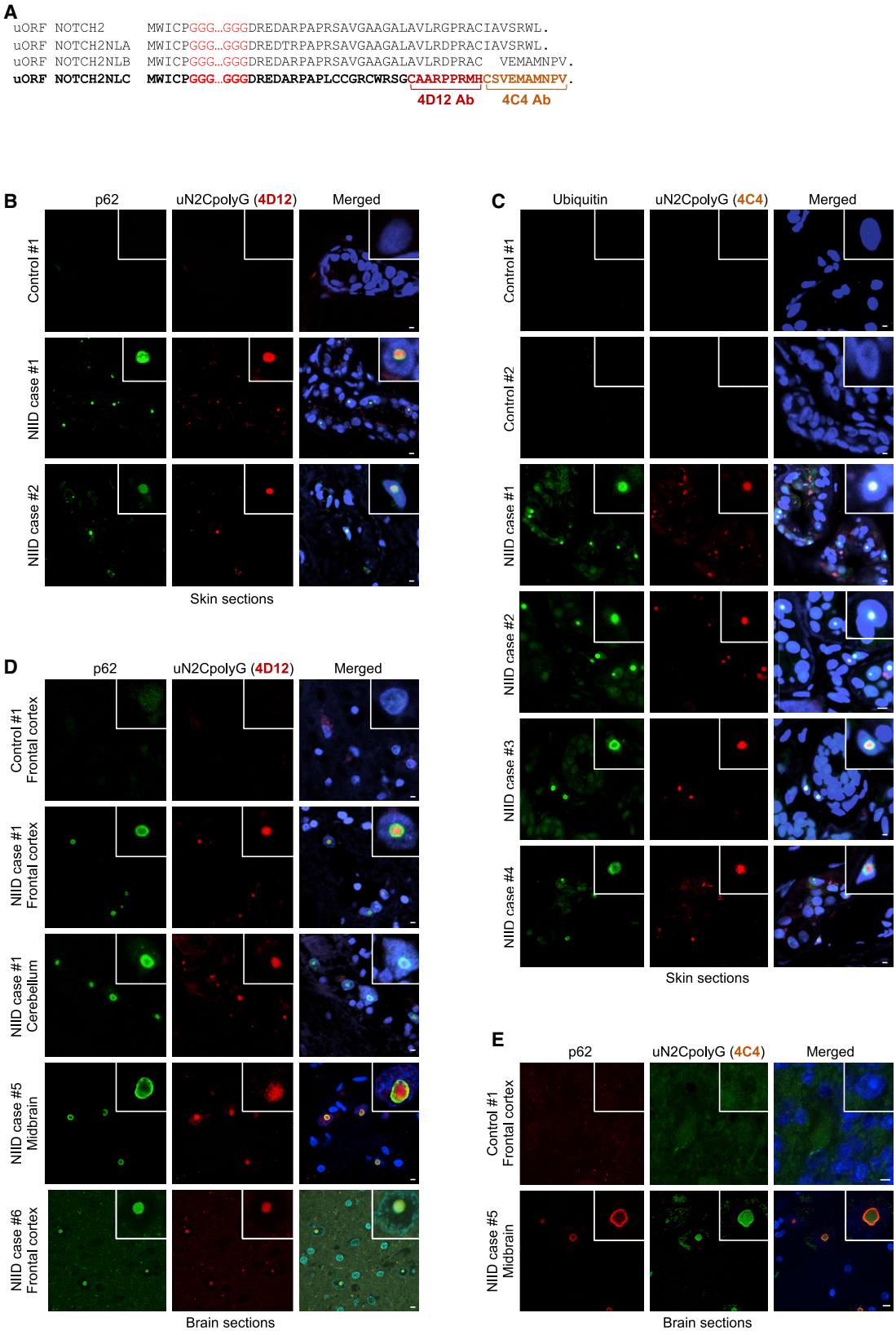

(legend on next page)

(Chen et al., 2020b). These unexpected results suggest that NIID is a heterogenous syndrome and that other mutations causing subtypes of this disorder remain to be identified, notably in European individuals with NIID.

Expression of uN2CpolyG is pathogenic in cells

To further study the uN2CpolyG protein, we cloned the full NOTCH2NLC uORF, from its ATG start codon in exon 1 to its penultimate codon in exon 2, containing its 38 C-terminal amino acids, with a control (12×) or an expanded (100×) size of GGC repeats, and fused this uN2C ORF to GFP or a hemagglutinin (HA) tag (Figure S3A). Cell transfection of the GFP-tagged N2C uORF with 12 or 100 GGC repeats indicated that their expression occurs independent of repeat size (Figure S3B). In contrast, fusion of the N2C uORF to a smaller HA tag (~1 kDa) resulted in detection of uN2CpolyG with 100 GGC repeats but limited expression with 12 repeats (Figures S3C and S3D). This is characteristic of short upstream ORFs that are translated into small and often unstable peptides that can be stabilized and detected when fused with a large tag such as GFP (Aspden et al., 2014). In support of this hypothesis, cell treatment with Bafilomycin A1, which inhibits the autophagy degradation pathway, increased expression of the small uN2C-HA protein with 12 GGC repeats (Figure S3D). These results suggest that translation of the N2C uORF occurs independent of the length of the GGC stretch. However, in absence of an expansion, the uN2C protein, like most uORF proteins, is small and unstable and, thus, expressed at low levels in control individuals, whereas uN2C is stabilized by the polyG expansion and accumulates in individuals with N2C NIID.

Next we investigated whether the uN2CpolyG protein could be responsible for the typical inclusions and the neuronal cell dysfunctions observed in NIID. Importantly, immunofluorescence analyses indicated that sole expression of the uN2CpolyG protein in embryonic mouse cortical neuronal cell cultures was sufficient to form cytoplasmic and intranuclear inclusions, which are p62-positive (Figure 3A). Inclusions formation is likely driven by the polyG expansion because expression of a pure polyG stretch (ATG polyG-GFP), deleted of any uN2C sequence, also forms p62-positive cellular inclusions (Figure 3A). Identical results were obtained in immortalized cell lines (Figures S3E–S3G). Further analyses indicated that accretion of uN2CpolyG into cellular aggregates is progressive and parallels its accumulation in the insoluble fraction of transfected cell lysates (Figures S3F and S3G). Because protein aggregates can be degraded by macroautophagy, we tested whether compounds known to activate this catabolic process may prevent accumulation of the uN2CpolyG protein. Interestingly, inhibition of the mammalian target of rapamycin (mTOR) kinase decreases uN2CpolyG accumulation (Figure 3B). Finally, expression of the uN2CpolyG protein is toxic and leads to neuronal cell death in embryonic mouse cortical neuronal cell cultures (Figure 3C) and in GT1-7 immortalized neuronal cells (Figure S3H). Importantly, expression of the uN2C protein with a control number of glycine repeats (GGC 12x) was not overtly toxic, whereas expression of a polyG stretch in isolation and deleted of any uN2C sequence was sufficient to cause cell death (Figures 3C and S3H). These data indicate that expression of uN2CpolyG is pathogenic in cell culture, with its polyG stretch driving aggregation and toxicity.

To further investigate the mechanism of uN2CpolyG toxicity, we searched for potential proteins interacting with it. Cell transfection of uN2CpolyG-GFP followed by GFP immunoprecipitation and MS identified various associated proteins with clear enrichment for the Ku70 and Ku80 proteins (Figure S4A; Table S2). Ku70 and Ku80 form a heterodimeric ring that initiates nonhomologous DNA end joining (NHEJ) repair at DNA double-strand breaks (Grundy et al., 2014; Fell and Schild-Poulter, 2015). Co-immunoprecipitation confirmed that the control uN2C and uN2CpolyG proteins interact with the endogenous Ku proteins (Figure S4B). However, this interaction is independent of the glycine stretch because ku70 and Ku80 interact neither with the polyG-containing protein expressed in FXTAS (FMRpolyG) nor with a pure polyG stretch (ATG polyG-GFP) (Figure S4B). Mutation analyses of the uN2C ORF revealed that a central amino acid sequence that is absent from NOTCH2, NOTCH2NLA, and NOTCH2NLB putative upstream ORFs is essential for the interaction of uN2C with the Ku proteins (Figure S4C). Next we investigated localization of the uN2C and uN2CpolyG proteins upon induction of DNA damage. Interestingly, most of uN2CpolyG was immobilized in inclusions, with little protein recruited to sites of DNA damage (Figure S4D). In contrast, the control uN2C protein was recruited within second to sites of laser microirradiation-induced DNA damage. Mutation analyses indicated that this recruitment is dependent on the uN2C amino acid sequence required to interact with the Ku proteins (Figure S4D). These data suggest that the 5′ UTR of NOTCH2NLC contains an upstream ORF that encodes a small protein, uN2C, which binds to the Ku proteins and is recruited at DNA damage sites. In contrast, upon GGC repeat expansion, uN2C encodes a mutant polyG-containing protein, uN2CpolyG, which is immobilized in aggregates and, thus, cannot join DNA damage. These data question whether uN2C or uN2polyG may affect DNA repair. Immunoblotting and immunofluorescence against phospho-Ser139 H2AX (γH2AX), a marker of DNA double-strand breaks, indicated faster kinetics of DNA repair in irradiated cells expressing the uN2C control protein with 12 glycine as compared to control cells (Figures S4E and S4F). In contrast, the polyG expansion in uN2C leads to an inactive protein that is unable to promote DNA repair (Figures S4E and S4F). We thus tested whether this impaired activity may translate into any

Figure 2. The uN2polyG protein is present in NIID intranuclear inclusions

(A) Alignment of NOTCH2 and NOTCH2NLA, NOTCH2NLB, and NOTCH2NLC putative upstream ORFs. Brackets indicate the amino acid sequences against which the 4D12 and 4C4 antibodies are directed.

(B–E) Immunofluorescence against uN2CpolyG using 4D12 (B and D) or 4C4 (C and E) antibody and p62 (B, D, and E) or ubiquitin (C) on skin (B and C) and brain (D and E) sections of carriers of the *NOTCH2NLC*-GGC repeat expansion (N2C NIID) or age-matched control individuals. Scale bars, 10 μm. Nuclei were counterstained with DAPI.

See also Figure S2 and Table S1.

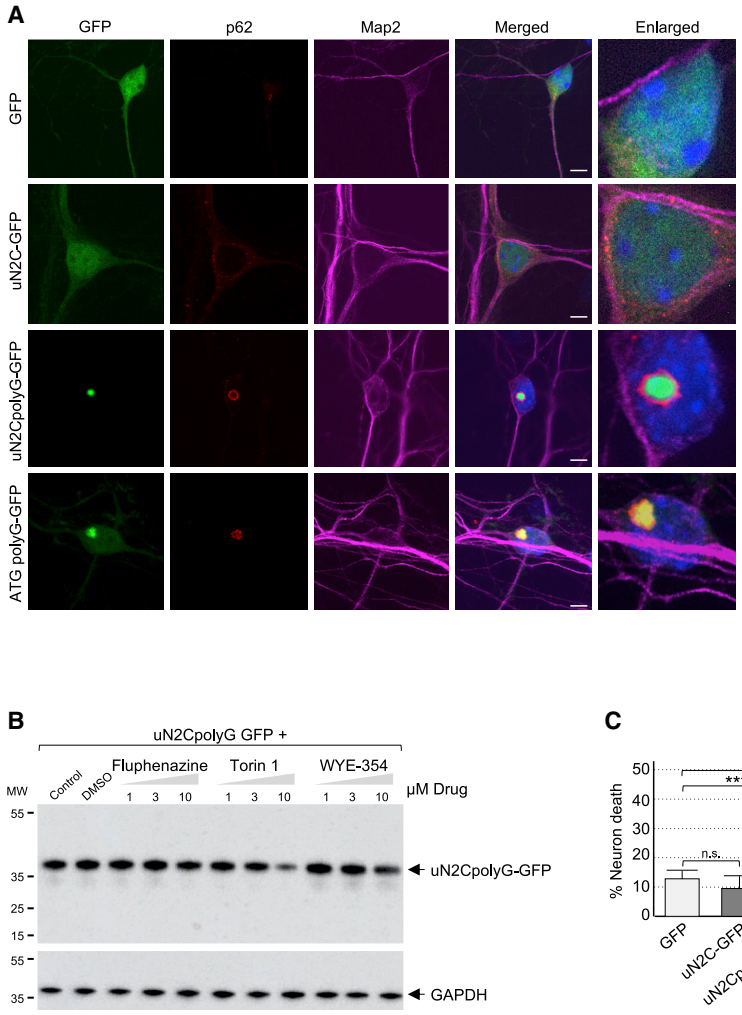

Figure 3. Expression of uN2CpolyG is toxic in cell culture

(A) GFP fluorescence and immunofluorescence against p62 and Map2 of cortical neuronal cell cultures from mouse embryos transduced for 24 h with GFP, uN2C-GFP (12 GGC), uN2CpolyG-GFP (100 GGC), or ATG polyG-GFP (70 GGC) AAV2/PHP.eB. Scale bars, 10 μm. Nuclei were counterstained with DAPI.

(B) Immunoblot against GFP or the GAPDH of proteins extracted from uN2CpolyG-GFP-transfected HEK293 cells treated for 15 h with the indicated drugs.

(C) Cell viability of cortical neuronal cell cultures from mouse embryos transduced with GFP, uN2C-GFP, uN2CpolyG-GFP, or ATG polyG-GFP AAV2/PHP.eB. Error bars indicate SEM. Student's t test, ***$p < 0.001$.

See also Figures S3, S4, and Table S2.

pathological consequences in NIID. However, immunofluorescence analyses revealed no overt mislocalization of the Ku proteins or any evident accumulation of γH2AX-positive DNA damage in uN2CpolyG-expressing cells or in skin and brain sections of individuals with adult-onset N2C NIID. These results indicate that the small uN2C protein is potentially a novel regulator of DNA damage response, whereas in NIID, a polyG expansion alters uN2C localization and DNA repair activity, but this reduced function is likely compensated by the second NOTCH2NLC allele and is not sufficient to drive overt DNA repair alterations in individuals with NIID.

Expression of uN2CpolyG is pathogenic in animals

To evaluate the pathological consequences of uN2polyG expression in animals, we injected mice with adeno-associated virus (AAV) particles expressing GFP-tagged uN2C with a control (12×) or pathogenic (100×) size of polyG. To target the central nervous system, we used an AAV serotype (PHP.eB) that crosses the blood-brain barrier upon intravenous injection. Furthermore, to focus on polyG protein toxicity and exclude any potential RNA gain-of-function mechanism, the GGC repeat sequence was modified to include alternative codons (GGA, GGT, and GGG) that also encode for glycine and, thus, avoid production of a pure GGC RNA hairpin. qRT-PCR indicated similar levels of expression between AAV GFP-, control uN2C-GFP-, and uN2CpolyG-GFP-injected mice (Figure S5A). To determine the consequences of uN2CpolyG production in mice, we conducted a series of locomotor assays. Three months after AAV injection, we noted a progressive alteration of motor performance and coordination of uN2CpolyG-expressing mice. First, AAV uN2CpolyG-injected mice were unable to sustain hindlimb extension under tail suspension compared with control AAV GFP- or uN2C-injected mice (Figure 4A). Furthermore, uN2CpolyG-expressing mice had an increased likelihood of falling from a rotarod (Figure 4B), showing increased foot faults and slips on a notched bar (Figure 4C; Videos S1, S2, and S3), and were hyperactive in the open field arena (Figure 4C) compared with control mice expressing the GFP or N2C uORF with a normal size of GGC repeats. These alterations likely originate from specific neuronal dysfunction and not from global health deterioration because animals expressing the uN2CpolyG protein were overall healthy with normal grip strength and normal weight (Figures S5B and S5C). We noted none of these locomotor changes 1.5 months after AAV injection, demonstrating that these alterations are progressive. Finally, expression of the polyG protein is deleterious because mice expressing uN2CpolyG die around 4–6 months after injection, whereas GFP- and control uN2C-injected mice exhibit normal longevity and are indistinguishable from control non-injected mice (Figure 4E). Importantly, expression of uN2CpolyG in mice leads to widespread formation of intranuclear inclusions, which are p62-, ubiquitin-, and sumo-positives (Figures 4F, 4G, and S5D–S5F), reproducing the characteristic histopathological features of NIID. Finally, we observed

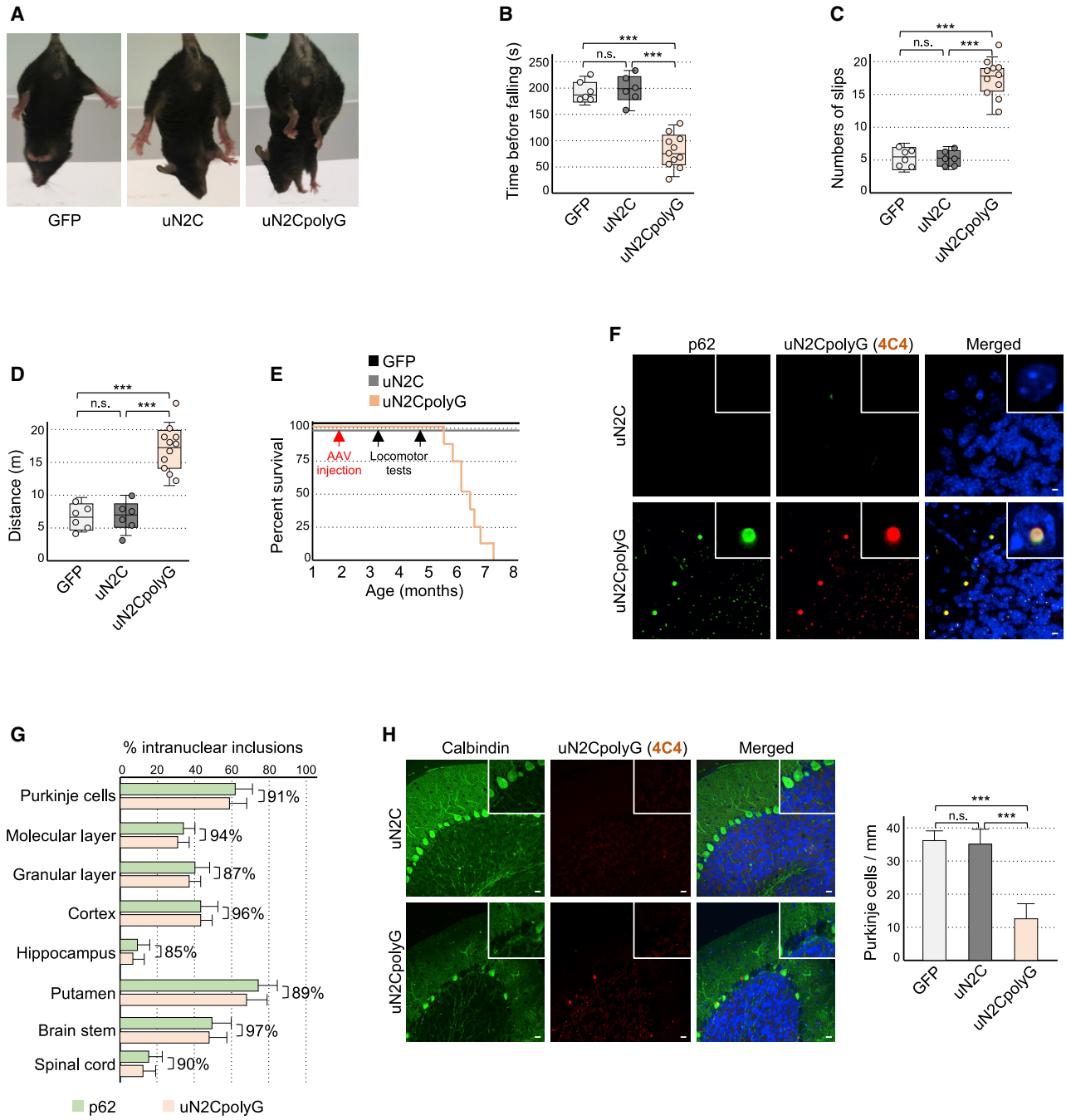

Figure 4. Expression of uN2CpolyG is pathogenic in animals

(A) 60-s tail suspension test shows hind limb clasping in uN2CpolyG-GFP-expressing mice compared with GFP or uN2C-GFP control animals.

(B–D) Time before falling from a rotating rod (B), numbers of paw slips and errors in the notched bar test (C), and maximal distance traveled during 30 min in an open field (D) for AAV2/PHP.eB GFP-injected (n = 6), uN2C-GFP-injected (n = 6), and uN2CpolyG-GFP-injected (n = 11) male mice tested 3 months after injection.

(E) Kaplan-Meier survival curve of AAV2/PHP.eB GFP-injected (n = 6), uN2C-GFP-injected (n = 6), and uN2CpolyG-GFP-injected (n = 8) male mice. Dates of AAV injection and locomotor tests are indicated by arrows.

(F) Immunofluorescence against uN2CpolyG and p62 on cerebellum areas of uN2C-GFP- and uN2CpolyG-GFP-expressing mice sacrificed 2 months after AAV injection. Scale bars, 10 μm.

(G) Quantification of p62- or uN2CpolyG-positive intranuclear inclusions in different brain regions of uN2CpolyG-GFP-expressing mice. Brackets indicate the percentage of co-localization between p62- and uN2polyG-positive intranuclear inclusions. N = 3 mice; at least 200 nuclei were counted per brain region and per animal.

(legend continued on next page)

neuronal cell death, notably loss of Purkinje cells, in mice expressing the uN2CpolyG protein (Figures 4H and S5G), which is consistent with the progressive loss of motor balance and coordination observed in these animals (Figures 4B and 4C; Videos S1, S2, and S3). Consistent with neurodegeneration, Gfap staining indicated increased neuroinflammation in brain sections of uN2CpolyG-injected mice (Figure S5H). Overall, these data suggest that expression of the uN2CpolyG protein in animals is toxic and is sufficient to generate the typical NIID intranuclear inclusions (Figure S6).

DISCUSSION

NIID is a rare neurodegenerative disorder caused by an expansion of GGC repeats located in the 5′ UTR of the NOTCH2NLC gene (Sone et al., 2019; Ishiura et al., 2019; Deng et al., 2019; Tian et al., 2019). The NOTCH2NLA, NOTCH2NLB, and NOTCH2NLC genes reside in the 1q21.1 locus and result from partial duplication of the NOTCH2 N-terminal part, which encodes six epidermal growth factor (EGF)-like domains but excludes NOTCH2 peptide signal, transmembrane, and cytoplasmic domains. Important for hominid brain size evolution, NOTCH2NL proteins regulate Notch signaling and expand human cortical progenitors (Fiddes et al., 2018; Suzuki et al., 2018). Furthermore, genomic duplications or deletions encompassing the NOTCH2NLA and/ or NOTCH2NLB genes lead to neurodevelopmental syndromes, whereas a GGC expansion in the NOTCH2NLC gene causes a neurodegenerative disease. These results highlight the importance of the *NOTCH2NL* gene for neuronal cells in humans but question how a repeat expansion embedded in a sequence predicted to be "non-coding" can be pathogenic.

Here we found that the NOTCH2NLC GGC repeats are embedded in a small upstream ORF, resulting in their translation into a polyG-containing protein that forms intranuclear inclusions and is toxic in cell and animal models (Figure S6). Immunoblotting and direct GFP observation indicate that NOTCH2NLC GGC repeats are mainly translated in the glycine frame through canonical initiation at an AUG start codon, but these assays may not be sensitive enough to detect low levels of polyA or polyR-containing proteins translated from non-canonical translation initiation in the repeats; thus, a contribution of RAN translation in NIID cannot be formally excluded. Translation of a small upstream ORF containing an expansion of GGC repeats into a toxic polyG protein is reminiscent of another neurodegenerative disorder, FXTAS, which is caused by an expansion of 70–200 CGG repeats located in the 5′ UTR of the *FMR1* gene (Hagerman et al., 2001). These repeats are embedded in a short upstream ORF that is translated through canonical initiation at an ACG near-cognate start codon into a polyG-containing protein, FMRpolyG, which, like uN2CpolyG, forms p62-positive intranuclear inclusions and causes neuronal cell death in cell and animal models (Todd et al., 2013; Hukema et al., 2015; Sellier et al., 2017). NIID and FXTAS share some common clinical features and quasi-indistinguishable histopathological characteristics with remarkably similar intranuclear inclusions (Gelpi et al., 2017; Lim et al., 2020). Thus, like neurodegenerative polyQ diseases, which are caused by CAG repeat expansions embedded in diverse ORFs that are translated into toxic polyglutamine-containing proteins, we propose that NIID and FXTAS represent a novel class of disorders, polyG diseases, where expansions of GGC repeats embedded in diverse upstream ORFs are translated into toxic polyG-containing proteins (Figure S6). Of interest, GGC repeat expansions located in the 5′ UTRs of the *LRP12*, *GIPC1*, and *NUTM2E* (also known as FAM22E) genes have been recently identified as the cause of the OPDM and OPML neuromuscular and neurodegenerative disorders (Ishiura et al., 2019; Deng et al., 2020; Xi et al., 2021). OPDM and OPML share some overlapping symptoms and similar histopathological features with NIID and FXTAS. Furthermore, GGC repeat expansions in NOTCH2NLC have been identified recently in individuals with oculopharyngodistal myopathy with neurological symptoms, highlighting the overlap between these diseases (Ogasawara et al., 2020; Yu et al., 2021). Whether these newly identified diseases caused by GGC repeats are pathogenic through a common mechanism, translation of ill-defined short upstream ORFs into toxic polyG-containing proteins that form intranuclear inclusions, is an exciting question for the future (Figure S6).

Another topic of discussion is the relationship between GGC repeat length and clinical features. In polyQ diseases, a clear correlation exists between the size of the CAG repeat expansion and the age of onset and disease severity. In NIID, it is noteworthy that intermediate sizes (40–80) of NOTCH2NLC GGC repeats increased the susceptibility to develop the parkinsonism-dominant form of NIID and were found recently in individuals with Parkinson's disease (Ma et al., 2020), whereas carriers of longer GGC expansions are more at risk to develop the dementia- and muscle weakness-dominant forms of NIID (Sone et al., 2019; Ishiura et al., 2019; Deng et al., 2019; Tian et al., 2019). However, an unambiguous correlation between repeat size and clinical severity might be limited to a narrow interval for 5′ UTR-embedded GGC repeat diseases because large expansions may trigger a potential "protective" mechanism because of their potential methylation and close proximity with promoters. Indeed, expansions over 200 CGG repeats in the 5′ UTR of the X-linked *FMR1* gene promote epigenetic DNA changes that silence *FMR1* promoter, resulting in decreased expression of the uORF encoding the toxic FMRpolyG protein but also in decreased expression of the main ORF encoding the synaptically important FMRP protein, whose loss cannot be compensated by a second allele in males, ultimately causing the

(H) Left panel: immunofluorescence against uN2CpolyG and calbindin on the cerebellum of uN2C-GFP- and uN2CpolyG-GFP-expressing mice sacrificed 4 months after AAV injection. Scale bars, 20 μm. Right panel: quantification of Purkinje cell numbers in GFP-expressing (n = 4), uN2C-GFP-expressing (n = 4), or uN2CpolyG-GFP-expressing (n = 4) mice.

In box-and-whisker plots, box upper and lower limits represent the 25th and 75th percentiles, whiskers represent minimum and maximum values, and a horizontal line across the box represents the median. Bar graphs indicate standard error of the mean (SEM). Student's t test, ***$p < 0.001$. Nuclei were counterstained with DAPI.

See also Figures S5 and S6 and Videos S1, S2, and S3.

neurodevelopmental fragile X syndrome (FXS). In NIID, if large GGC repeat expansions promote similar epigenetic changes, then this would result in silencing of the NOTCH2NLC allele carrying the GGC expansion, abolishing expression of the toxic uN2CpolyG protein, whereas decreased expression of the main ORF encoding the N2C protein would be likely non-pathogenic, as compensated by the second NOTCH2NLC allele. In short, because of a potential "protective" transcriptional silencing mechanism promoted by a high number of repeats, it is possible that 5′ UTR-embedded GC-rich repeat diseases (FXTAS, NIID, OPDM, and OPML) may not systematically follow a classic autosomal dominant inheritance. This potential promoter silencing mechanism may also explain why these diseases do not show evident anticipation (increased severity and/or younger age of onset with increased number of repeats) over a certain threshold of repeats.

Regarding the potential mechanism of toxicity of these polyG proteins, how they cause cell death is unclear. We found that the control uN2C protein interacts with the Ku70 and Ku80 proteins and activates DNA repair. Expansion of the polyG stretch impairs uN2C localization and interaction with the Ku proteins, resulting in a NHEJ-inactive uN2CpolyG protein. Alterations of DNA repair mechanisms can lead to various neurodegenerative syndromes. However, potential haploinsufficiency of uN2C in NIID is unlikely because NOTCH2NLC mRNA levels are unaltered in NIID (Sone et al., 2019; Ishiura et al., 2019; Tian et al., 2019). Furthermore, individuals with NIID lack the typical sensitivity to ionizing radiation, immunodeficiency, and microcephaly observed in individuals with radiosensitivity with severe combined immunodeficiency (RS-SCID), who are carriers of loss-of-function mutations in components of the NHEJ repair mechanism (Woodbine et al., 2014). Finally, we do not observe overt mislocalization of the Ku proteins or accumulation of DNA damage in cell and animal models of NIID, nor in skin and brain sections of adult individuals with NIID. Similarly, we found neither alterations of the Ku proteins nor increased DNA damage in cells or mice expressing the FXTAS polyG-containing protein FMRpolyG. Thus, we believe that potential alteration of DNA repair is most likely not the main cause of neuronal cell death in NIID. In contrast, uN2CpolyG and FMRpolyG possess a common polyG stretch that, when expressed in isolation, is sufficient to form p62-positive inclusions and causes neuronal cell death. Formation of cellular inclusions is consistent with the known *in vitro* self-aggregation properties of polyG homopolypeptides, which form amyloid-like fibrils (Lorusso et al., 2011; Plumley et al., 2011), but the molecular and cellular mechanisms by which these polyG proteins move into cell nuclei and drive neuronal cell dysfunctions remain unknown.

These results unveil a novel class of genetic disorders, polyG diseases, in which expanded GGC repeats embedded in upstream ORFs are translated into toxic polyG-containing proteins. Pharmaceutical compounds modulating autophagy could be of therapeutic interest to prevent toxic accumulation of these proteins.

STAR★METHODS

Detailed methods are provided in the online version of this paper and include the following:

SUPPLEMENTAL INFORMATION

Supplemental information can be found online at https://doi.org/10.1016/j.neuron.2021.03.038.

ACKNOWLEDGMENTS

This work was supported by the National Natural Science Foundation of China (81571219, 82071409, and U20A20356 to Z.W.); the Double Thousand Talents Program of Jiangxi Province (to D.H.); the Peking University Medicine Fund of Fostering Young Scholars' Scientific & Technological Innovation (to J.D.); the Japan Society for the Promotion of Science (KAKENHI JP19H03577) and the MHLW FC Program (JPMH19189624) (to J.S.); ERC-2012-StG 310659, ANR-18-CE16-0019, and FRM EQU202103012936 (to N.C.B.); and ANR-10-LABX-0030-INRT and ANR-10-IDEX-0002-02 (to I.G.B.M.C.).

AUTHOR CONTRIBUTIONS

Experiments were performed by M.B., J.D., J.S., V.P., B.M., F. Ruffenach, F. Riet, E.G., P.K., H.J., and M.O.-A. Control and NIID cases originated from K.M., W.A.C., A.A.D., D.H., H.M., Y.I., J.S., and Z.W. Data were collected and analyzed by M.B., J.D., J.S., Z.W., W.A.C., A.A.D., E.G., L.N., and N.C.-B. The study was designed, coordinated, and written by N.C.-B. with input from all authors.

DECLARATION OF INTEREST

The authors declare no competing interests.

Received: August 8, 2020
Revised: January 8, 2021
Accepted: March 30, 2021
Published: April 21, 2021

SUPPORTING CITATIONS

The following references appear in the Supplemental information: Cupidi et al. (2019), McFadden et al. (2005).

REFERENCES

Aspden, J.L., Eyre-Walker, Y.C., Phillips, R.J., Amin, U., Mumtaz, M.A., Brocard, M., and Couso, J.P. (2014). Extensive translation of small Open Reading Frames revealed by Poly-Ribo-Seq. Elife *3*, e03528.

Chen, H., Lu, L., Wang, B., Cui, G., Wang, X., Wang, Y., Raza, H.K., Min, Y., Li, K., Cui, Y., et al. (2020a). Re-defining the clinicopathological spectrum of neuronal intranuclear inclusion disease. Ann. Clin. Transl. Neurol. *7*, 1930–1941.

Chen, Z., Yan Yau, W., Jaunmuktane, Z., Tucci, A., Sivakumar, P., Gagliano Taliun, S.A., Turner, C., Efthymiou, S., Ibáñez, K., Sullivan, R., et al.; Genomics England Research Consortium (2020b). Hardy J, Ryten M, Vandrovcova J, Houlden H. Neuronal intranuclear inclusion disease is genetically heterogeneous. Ann. Clin. Transl. Neurol. *7*, 1716–1725.

Cortese, A., Simone, R., Sullivan, R., Vandrovcova, J., Tariq, H., Yau, W.Y., Humphrey, J., Jaunmuktane, Z., Sivakumar, P., Polke, J., et al. (2019). Biallelic expansion of an intronic repeat in RFC1 is a common cause of late-onset ataxia. Nat. Genet. *51*, 649–658.

Cupidi, C., Dijkstra, A.A., Melhem, S., Vernooij, M.W., Severijnen, L.A., Hukema, R.K., Rozemuller, A.J.M., Neumann, M., van Swieten, J.C., and Seelaar, H. (2019). Refining the Spectrum of Neuronal Intranuclear Inclusion Disease: A Case Report. J. Neuropathol. Exp. Neurol. *78*, 665–670.

Deng, J., Gu, M., Miao, Y., Yao, S., Zhu, M., Fang, P., Yu, X., Li, P., Su, Y., Huang, J., et al. (2019). Long-read sequencing identified repeat expansions in the 5'UTR of the *NOTCH2NLC* gene from Chinese patients with neuronal intranuclear inclusion disease. J. Med. Genet. *56*, 758–764.

Deng, J., Yu, J., Li, P., Luan, X., Cao, L., Zhao, J., Yu, M., Zhang, W., Lv, H., Xie, Z., et al. (2020). Expansion of GGC Repeat in GIPC1 Is Associated with Oculopharyngodistal Myopathy. Am. J. Hum. Genet. *106*, 793–804.

Fang, P., Yu, Y., Yao, S., Chen, S., Zhu, M., Chen, Y., Zou, K., Wang, L., Wang, H., Xin, L., et al. (2020). Repeat expansion scanning of the NOTCH2NLC gene in patients with multiple system atrophy. Ann. Clin. Transl. Neurol. *7*, 517–526.

Fell, V.L., and Schild-Poulter, C. (2015). The Ku heterodimer: function in DNA repair and beyond. Mutat. Res. Rev. Mutat. Res. *763*, 15–29.

Fiddes, I.T., Lodewijk, G.A., Mooring, M., Bosworth, C.M., Ewing, A.D., Mantalas, G.L., Novak, A.M., van den Bout, A., Bishara, A., Rosenkrantz, J.L., et al. (2018). Human-Specific NOTCH2NL Genes Affect Notch Signaling and Cortical Neurogenesis. Cell *173*, 1356–1369.e22.

Gao, F.B., and Richter, J.D. (2017). Microsatellite Expansion Diseases: Repeat Toxicity Found in Translation. Neuron *93*, 249–251.

Gelpi, E., Botta-Orfila, T., Bodi, L., Marti, S., Kovacs, G., Grau-Rivera, O., Lozano, M., Sánchez-Valle, R., Muñoz, E., Valldeoriola, F., et al. (2017). Neuronal intranuclear (hyaline) inclusion disease and fragile X-associated tremor/ataxia syndrome: a morphological and molecular dilemma. Brain *140*, e51.

Grundy, G.J., Moulding, H.A., Caldecott, K.W., and Rulten, S.L. (2014). One ring to bring them all–the role of Ku in mammalian non-homologous end joining. DNA Repair (Amst.) *17*, 30–38.

Hagerman, R.J., Leehey, M., Heinrichs, W., Tassone, F., Wilson, R., Hills, J., Grigsby, J., Gage, B., and Hagerman, P.J. (2001). Intention tremor, parkinsonism, and generalized brain atrophy in male carriers of fragile X. Neurology *57*, 127–130.

Hukema, R.K., Buijsen, R.A., Schonewille, M., Raske, C., Severijnen, L.A., Nieuwenhuizen-Bakker, I., Verhagen, R.F., van Dessel, L., Maas, A., Charlet-Berguerand, N., et al. (2015). Reversibility of neuropathology and motor deficits in an inducible mouse model for FXTAS. Hum. Mol. Genet. *24*, 4948–4957.

Ishiura, H., and Tsuji, S. (2020). Advances in repeat expansion diseases and a new concept of repeat motif-phenotype correlation. Curr. Opin. Genet. Dev. *65*, 176–185.

Ishiura, H., Shibata, S., Yoshimura, J., Suzuki, Y., Qu, W., Doi, K., Almansour, M.A., Kikuchi, J.K., Taira, M., Mitsui, J., et al. (2019). Noncoding CGG repeat expansions in neuronal intranuclear inclusion disease, oculopharyngodistal myopathy and an overlapping disease. Nat. Genet. *51*, 1222–1232.

Li, M., Li, K., Li, X., Tian, Y., Shen, L., Wu, G., Zhang, Z., and Chen, W. (2020). Multiple reversible encephalitic attacks: a rare manifestation of neuronal intranuclear inclusion disease. BMC Neurol. *20*, 125.

Lim, S.Y., Ishiura, H., Ramli, N., Shibata, S., Almansour, M.A., Tan, A.H., Houlden, H., Lang, A.E., and Tsuji, S. (2020). Adult-onset neuronal intranuclear inclusion disease mimicking Fragile X-associated tremor-ataxia syndrome in ethnic Chinese patients. Parkinsonism Relat. Disord. *74*, 25–27.

Lindenberg, R., Rubinstein, L.J., Herman, M.M., and Haydon, G.B. (1968). A light and electron microscopy study of an unusual widespread nuclear inclusion body disease. A possible residuum of an old herpesvirus infection. Acta Neuropathol. *10*, 54–73.

Liu, Y., Mimuro, M., Yoshida, M., Hashizume, Y., Niwa, H., Miyao, S., Ujihira, N., and Akatsu, H. (2008). Inclusion-positive cell types in adult-onset intranuclear inclusion body disease: implications for clinical diagnosis. Acta Neuropathol. *116*, 615–623.

Lorusso, M., Pepe, A., Ibris, N., and Bochicchio, B. (2011). Molecular and supramolecular studies on polyglycine and poly-l-proline. Soft Matter *7*, 6327.

Ma, D., Tan, Y.J., Ng, A.S.L., Ong, H.L., Sim, W., Lim, W.K., Teo, J.X., Ng, E.Y.L., Lim, E.C., Lim, E.W., et al. (2020). Association of NOTCH2NLC Repeat Expansions With Parkinson Disease. JAMA Neurol. *77*, 1–5.

McFadden, K., Hamilton, R.L., Insalaco, S.J., Lavine, L., Al-Mateen, M., Wang, G., and Wiley, C.A. (2005). Neuronal intranuclear inclusion disease without polyglutamine inclusions in a child. J. Neuropathol. Exp. Neurol. *64*, 545–552.

Mori, F., Tanji, K., Odagiri, S., Hattori, M., Hoshikawa, Y., Kono, C., Yasui, K., Yokoi, S., Hasegawa, Y., Kamitani, T., et al. (2012). Ubiquitin-related proteins in neuronal and glial intranuclear inclusions in intranuclear inclusion body disease. Pathol. Int. *62*, 407–411.

Munoz-Garcia, D., and Ludwin, S.K. (1986). Adult-onset neuronal intranuclear hyaline inclusion disease. Neurology *36*, 785–790.

Nakamura, M., Murray, M.E., Lin, W.L., Kusaka, H., and Dickson, D.W. (2014). Optineurin immunoreactivity in neuronal and glial intranuclear inclusions in adult-onset neuronal intranuclear inclusion disease. Am. J. Neurodegener. Dis. *3*, 93–102.

Nelson, D.L., Orr, H.T., and Warren, S.T. (2013). The unstable repeats–three evolving faces of neurological disease. Neuron *77*, 825–843.

Ogasawara, M., Iida, A., Kumutpongpanich, T., Ozaki, A., Oya, Y., Konishi, H., Nakamura, A., Abe, R., Takai, H., Hanajima, R., et al. (2020). CGG expansion in NOTCH2NLC is associated with oculopharyngodistal myopathy with neurological manifestations. Acta Neuropathol. Commun. *8*, 204.

Plumley, J.A., Tsai, M.I., and Dannenberg, J.J. (2011). Aggregation of capped hexaglycine strands into hydrogen-bonding motifs representative of pleated and rippled β-sheets, collagen, and polyglycine I and II crystal structures. A density functional theory study. J. Phys. Chem. B *115*, 1562–1570.

Pountney, D.L., Huang, Y., Burns, R.J., Haan, E., Thompson, P.D., Blumbergs, P.C., and Gai, W.P. (2003). SUMO-1 marks the nuclear inclusions in familial neuronal intranuclear inclusion disease. Exp. Neurol. *184*, 436–446.

Rafehi, H., Szmulewicz, D.J., Bennett, M.F., Sobreira, N.L.M., Pope, K., Smith, K.R., Gillies, G., Diakumis, P., Dolzhenko, E., Eberle, M.A., et al. (2019). Bioinformatics-Based Identification of Expanded Repeats: A Non-reference Intronic Pentamer Expansion in RFC1 Causes CANVAS. Am. J. Hum. Genet. *105*, 151–165.

Rodriguez, C.M., and Todd, P.K. (2019). New pathologic mechanisms in nucleotide repeat expansion disorders. Neurobiol. Dis. *130*, 104515.

Sellier, C., Buijsen, R.A.M., He, F., Natla, S., Jung, L., Tropel, P., Gaucherot, A., Jacobs, H., Meziane, H., Vincent, A., et al. (2017). Translation of Expanded CGG Repeats into FMRpolyG Is Pathogenic and May Contribute to Fragile X Tremor Ataxia Syndrome. Neuron *93*, 331–347.

Sone, J., Hishikawa, N., Koike, H., Hattori, N., Hirayama, M., Nagamatsu, M., Yamamoto, M., Tanaka, F., Yoshida, M., Hashizume, Y., et al. (2005). Neuronal intranuclear hyaline inclusion disease showing motor-sensory and autonomic neuropathy. Neurology *65*, 1538–1543.

Sone, J., Tanaka, F., Koike, H., Inukai, A., Katsuno, M., Yoshida, M., Watanabe, H., and Sobue, G. (2011). Skin biopsy is useful for the antemortem

diagnosis of neuronal intranuclear inclusion disease. Neurology *76*, 1372–1376.

Sone, J., Kitagawa, N., Sugawara, E., Iguchi, M., Nakamura, R., Koike, H., Iwasaki, Y., Yoshida, M., Takahashi, T., Chiba, S., et al. (2014). Neuronal intranuclear inclusion disease cases with leukoencephalopathy diagnosed via skin biopsy. J. Neurol. Neurosurg. Psychiatry *85*, 354–356.

Sone, J., Mori, K., Inagaki, T., Katsumata, R., Takagi, S., Yokoi, S., Araki, K., Kato, T., Nakamura, T., Koike, H., et al. (2016). Clinicopathological features of adult-onset neuronal intranuclear inclusion disease. Brain *139*, 3170–3186.

Sone, J., Mitsuhashi, S., Fujita, A., Mizuguchi, T., Hamanaka, K., Mori, K., Koike, H., Hashiguchi, A., Takashima, H., Sugiyama, H., et al. (2019). Long-read sequencing identifies GGC repeat expansions in NOTCH2NLC associated with neuronal intranuclear inclusion disease. Nat. Genet. *51*, 1215–1221.

Sun, Q.Y., Xu, Q., Tian, Y., Hu, Z.M., Qin, L.X., Yang, J.X., Huang, W., Xue, J., Li, J.C., Zeng, S., et al. (2020). Expansion of GGC repeat in the human-specific NOTCH2NLC gene is associated with essential tremor. Brain *143*, 222–233.

Suzuki, I.K., Gacquer, D., Van Heurck, R., Kumar, D., Wojno, M., Bilheu, A., Herpoel, A., Lambert, N., Cheron, J., Polleux, F., et al. (2018). Human-Specific NOTCH2NL Genes Expand Cortical Neurogenesis through Delta/Notch Regulation. Cell *173*, 1370–1384.e16.

Takahashi-Fujigasaki, J. (2003). Neuronal intranuclear hyaline inclusion disease. Neuropathology *23*, 351–359.

Takahashi-Fujigasaki, J., Nakano, Y., Uchino, A., and Murayama, S. (2016). Adult-onset neuronal intranuclear hyaline inclusion disease is not rare in older adults. Geriatr. Gerontol. Int. *16* (*Suppl 1*), 51–56.

Tian, Y., Wang, J.L., Huang, W., Zeng, S., Jiao, B., Liu, Z., Chen, Z., Li, Y., Wang, Y., Min, H.X., et al. (2019). Expansion of Human-Specific GGC Repeat in Neuronal Intranuclear Inclusion Disease-Related Disorders. Am. J. Hum. Genet. *105*, 166–176.

Todd, P.K., Oh, S.Y., Krans, A., He, F., Sellier, C., Frazer, M., Renoux, A.J., Chen, K.C., Scaglione, K.M., Basrur, V., et al. (2013). CGG repeat-associated translation mediates neurodegeneration in fragile X tremor ataxia syndrome. Neuron *78*, 440–455.

Woodbine, L., Gennery, A.R., and Jeggo, P.A. (2014). The clinical impact of deficiency in DNA non-homologous end-joining. DNA Repair (Amst.) *16*, 84–96.

Xi, J., Wang, X., Yue, D., Dou, T., Wu, Q., Lu, J., Liu, Y., Yu, W., Qiao, K., Lin, J., et al. (2021). 5′ UTR CGG repeat expansion in GIPC1 is associated with oculopharyngodistal myopathy. Brain *144*, 601–614.

Yu, J., Deng, J., Guo, X., Shan, J., Luan, X., Cao, L., Zhao, J., Yu, M., Zhang, W., Lv, H., et al. (2021). The GGC repeat expansion in NOTCH2NLC is associated with oculopharyngodistal myopathy type 3. Brain. Published online March 9, 2021. https://doi.org/10.1093/brain/awab077.

Yuan, Y., Liu, Z., Hou, X., Li, W., Ni, J., Huang, L., Hu, Y., Liu, P., Hou, X., Xue, J., et al. (2020). Identification of GGC repeat expansion in the *NOTCH2NLC* gene in amyotrophic lateral sclerosis. Neurology *95*, e3394–e3405.

Zu, T., Gibbens, B., Doty, N.S., Gomes-Pereira, M., Huguet, A., Stone, M.D., Margolis, J., Peterson, M., Markowski, T.W., Ingram, M.A., et al. (2011). Non-ATG-initiated translation directed by microsatellite expansions. Proc. Natl. Acad. Sci. USA *108*, 260–265.

STAR★METHODS

KEY RESOURCES TABLE

REAGENT or RESOURCE	SOURCE	IDENTIFIER
Antibodies		
Anti-uN2CpolyG (SVEMAMNPV), Mouse Monoclonal Clone 4C4	This paper	N/A
Anti-uN2CpolyG (AARPPRMH), Mouse Monoclonal Clone 4D12	This paper	N/A
Anti-FLAG (DYKDDDDK) tag, Rabbit Polyclonal,	Thermo Fisher Scientific	Cat# PA1-984B; RRID: AB_347227
Anti-HA (YPYDVPDYA) tag, Mouse Monoclonal Clone 16B12	Abcam	Cat# ab130275; RRID: AB_11156884
Anti-GFP, Rabbit Polyclonal,	Abcam	Cat# ab290; RRID: AB_303395
Anti-GAPDH, Mouse Monoclonal Clone GA1R	Abcam	Cat# ab125247; RRID: AB_11129118
Anti-Calbindin, Mouse Monoclonal Clone CB-955	Abcam	Cat# ab82812; RRID: AB_1658451
Anti-Ubiquitin, Rabbit Monoclonal Recombinant EPR8830	Abcam	Cat# ab134953; RRID: AB_2801561
Anti-Sumo 2 and 3, Rabbit Polyclonal	Abcam	Cat# ab3742; RRID: AB_304041
Anti-p62 (*SQSTM1*), Rabbit Monoclonal Recombinant EPR4844	Abcam	Cat# ab109012; RRID: AB_2810880
Anti-MAP2, Mouse Monoclonal Clone MT-01	Abcam	Cat# ab7756; RRID: AB_306050
Anti-Histone H2A.X phospho S139, Rabbit Monoclonal Recombinant EP854(2)Y	Abcam	Cat# ab81299; RRID: AB_1640564
Anti-Histone H2A.X, Rabbit Monoclonal Recombinant EPR22820-23	Abcam	Cat# ab229914
Anti-Ku80 (*XRCC5*), Mouse Monoclonal Clone 5C5	Abcam	Cat# ab119935; RRID: AB_10899161
Anti-Ku-70 (*XRCC6*), Mouse Monoclonal Clone N3H10	Santa Cruz Biotechnology	Cat# sc-56129; RRID: AB_794205
Anti-GFAP, Rabbit Polyclonal,	Proteintech	Cat# 16825-1-AP; RRID: AB_2109646
Bacterial and virus strains		
AAV2/PHP.eB CAG GFP	This paper	N/A
AAV2/PHP.eB CAG uN2C-GFP	This paper	N/A
AAV2/PHP.eB CAG uN2CpolyG-GFP	This paper	N/A
One Shot Stbl3 Chemically Competent *E. coli*	Invitrogen	Cat# C737303
One Shot TOP10 Chemically Competent *E. coli*	Invitrogen	Cat# C404003
Biological samples		
Human skin and brain tissues	Described in Table S1	N/A
Chemicals, peptides, and recombinant proteins		
Lysostaphin Enzyme Protein Recombinant	ProSpec	Cat# ENZ-269
Histosol Plus	LifeScience Products	Cat# HS-100-5GL
TO-PRO-3 Iodide (642/661) - 1 mM Solution in DMSO	Fisher Scientific	Cat# T-3605
Lipofectamine 2000 Transfection reagent	Fisher Scientific	Cat# 11668019
Complete Mini EDTA-free Protease Inhibitor Cocktail	Roche	Cat# 11836170001
Bafilomycin A1	Sigma	Cat# B1793
MG132	Sigma	Cat# M8699
Doxycycline hydrochloride	Sigma	Cat# D3447
Critical commercial assays		
Anti-GFP Magnetic beads	Abcam	Cat# ab193983
Anti-HA Magnetic Beads	Pierce	Cat# 88837
EC Prime Western Blotting Detection Reagent	Sigma	Cat# GERPN2236
DAB Substrate Kit	Abcam	Cat# ab64238
TRI Reagent (Guanidine Thiocyanate & Phenol)	Merck	Cat# T9424-25ML
Transcriptor High Fidelity cDNA Synthesis Kit	Sigma	Cat# 5081955001
LightCycler 480 SYBR Green I Master	Roche	Cat# 04707516001

(*Continued on next page*)

Continued

REAGENT or RESOURCE	SOURCE	IDENTIFIER
Experimental models: Cell lines		
Human: U2OS cells	ATCC	Cat# 300364/p489_U-2_OS; RRID: CVCL_0042
Human: HEK293 cells	ATCC	Cat# 300192/p777_HEK293; RRID: CVCL_0045
Mouse: GT1-7 cells	ATCC	Cat# SCC116; RRID: CVCL_0281
Human: U2OS T-REx TO-uN2C-GFP	This paper	N/A
Human: U2OS T-REx TO-uN2CpolyG-GFP	This paper	N/A
Experimental models: Organisms/strains		
Wild type Mouse: C57BL/6J *Mus musculus*	The Jackson, Laboratory	JAX:000664, RRID: IMSR_JAX:000664
Oligonucleotides		
Primer RT-qPCR GFP Forward ACGTAAACGGCCACAAGTTC	This paper	N/A
Primer RT-qPCR GFP Reverse AAGTCGTGCTGCTTCATGTG	This paper	N/A
Primer RT-qPCR *RPLP0* Forward GAAGTCACTGTGCCAGCCCA	This paper	N/A
Primer RT-qPCR *RPLP0* Reverse GAAGGTGTAATCCGTCTCCA	This paper	N/A
Recombinant DNA		
Plasmid: pcDNA3-TetOn uN2C-GFP (12 GLY)	This paper	N/A
Plasmid: pcDNA3-TetOn uN2CpolyG-GFP (100 GLY)	This paper	N/A
Plasmid: pAAV2-CAG uN2C-GFP (12 GLY)	This paper	N/A
Plasmid: pAAV2-CAG uN2CpolyG-GFP (100 GLY)	This paper	N/A
Plasmid: pcDNA3 *NOTCH2NLC* Exon1-GFP Gly frame	This paper	N/A
Plasmid: pcDNA3 *NOTCH2NLC* Exon1-GFP Ala frame	This paper	N/A
Plasmid: pcDNA3 *NOTCH2NLC* Exon1-GFP Arg frame	This paper	N/A
Plasmid: pcDNA3 ATG GLY 70x-GFP	This paper	N/A
Plasmid: pcDNA3 ATG ALA 100x-GFP	This paper	N/A
Plasmid: pcDNA3 ATG ARG 100x-GFP	This paper	N/A
Software and algorithms		
Fiji (ImageJ)	NIH	RRID: SCR_002285
Prism	GraphPad	RRID: SCR_005375

RESOURCE AVAILABILITY

Lead contact

Further information and requests for resources and reagents should be directed to and will be fulfilled by the Lead Contact, Nicolas Charlet-Berguerand (ncharlet@igbmc.fr).

Materials availability

All unique reagents (e.g., uN2CpolyG constructs, 4C4 and 4D12 antibodies, etc.) generated in this study are available from the Lead Contact under MTA subject to restrictions from commercial source.

Data and code availability

Proteomics datasets related to Figure S4 in the paper are available in Table S2. Complete proteomics source data are available from the corresponding author upon reasonable request. No further unique datasets or codes were generated in this study.

EXPERIMENTAL MODEL AND SUBJECT DETAILS

Human samples

Patient available information is described in Table S1. Human skin and brain samples were sampled with the informed consent of individuals and families and approved by the Institutional Review Board of the Peking University First Hospital and Suzuka National Hospital.

Mice

All animal work was performed with approval from the IGBMC/ICS Animal Care Committee and of the French agency for research on animal (DGRI) authorization number APAFIS#11459-2017092208308760. C57BL/6 wild-type male mice were retro-orbitally AAV-injected at 2 months and then housed for 6 to 8 months in a temperature-controlled room (19–22°C) with a 12:12-hours light/dark cycle and free access to food and water. Mice were sacrificed by cervical dislocation in order to dissect the brain and spinal cord which were subsequently frozen for molecular biology or PFA-fixed and embedded in paraffin for histology.

Cell cultures and models

Mouse primary cortical neurons were prepared from E18 C57BL/6 wild-type mice embryos. Cortical regions were dissected and digested in 1X HBSS (ThermoFisher) with 0.25% trypsin (ThermoFisher) at 37°C for 10 minutes. Trypsin digestion was stopped by addition of DMEM (ThermoFisher), 10% horse serum (Life Technologies) and 1x GlutaMAX (ThermoFisher). Then, cortical neurons were dissociated, centrifuged, resuspended and plated on 0.1 mg/ml poly L-lysine (Sigma) pre-coated 24-well plates in Neurobasal Medium (ThermoFisher) supplemented with 1x B27, 0.5 mM L-glutamine and 100 IU/ml penicillin/streptomycin (ThermoFisher) at 37°C with 5% CO2. Neuronal GT1-7 cells were grown in DMEM 4.5 g/l glucose with 10% fetal calf serum and 100 IU/ml penicillin/streptomycin at 37°C in 5% CO2. U2OS and HEK293 cells were grown in DMEM 1 g/l glucose with 10% FCS and gentamycin at 37°C in 5% CO2. U2OS T-REx cells (ThermoFisher) stably expressing uN2C-GFP or uN2CpolyG-GFP were Lipofectamine-transfected with Pci1-linearized pcDNA3-TetOn expressing uN2C with 12 or 100 optimized GGC fused to the GFP and sectioned for neomycin resistance for two weeks.

METHOD DETAILS

Constructs

Human NOTCH2NLC exon 1 sequence containing 166 nts upstream of the GGC repeats was cloned into pcDNA3.1 fused to a the GFP deleted of its ATG and in all three frames. Mutations of the repeats size, ATG start codon or within the uN2C ORF were achieved by inverse PCR or by oligonucleotide ligations. NOTCH2NLC upstream ORF fused to the GFP with either 12 or 100 optimized GGN repeats was cloned into the pcDNA3-TetOn and pAAV2-CAG vector. To insure stability of repeat expansions, all GGC repeat-containing plasmids were transformed into STBL3 bacterial strain (Invitrogen). All constructs were confirmed by sanger sequencing.

Cell transfection and treatments

For AAV transduction of mouse primary cortical neurons, 4 to 5 days differentiated mouse primary cortical neurons were incubated with 5x10EXP10 vg/ml of AAV2/PHP.eB expressing the GFP, uN2C-GFP or uN2CpolyG-GFP, half of the media was changed every 48 hours and cells were let differentiated for 4 to 6 more days. For transient transfection, cells were plated in DMEM and 0.1% fetal bovine serum and transfected for 24 hours using Lipofectamine 2000 (Fisher Scientific). After 1 to 6 days post transient transfection, induction with 1 μg/mL doxycycline (Sigma) or AAV transduction, cells were analyzed by immunofluorescence or western blotting. For cell viability, mouse cortical neurons primary cultures were incubated 10 min with 1 μg/ml of propidium iodide and analyzed by microscopy. For GT1-7 cell viability, cells were detached by trypsin and resuspended in PBS with 20 nM TO-PRO-3 iodide (Fisher scientific) and FACS analyzed. Cells were treated with 100 nM of Bafilomycin A1, 1 μM MG132 or the indicated concentration of drug (Sigma) during 15 hours before analysis.

Mass spectrometry analysis

HEK293 cells were transfected with uN2C-GFP plasmid using Lipofectamine 2000 (Fisher Scientific) for 24 hours. Proteins were purified by GFP-immunoprecipitation, trypsin digested and the peptides were extracted twice with acetonitrile/water/formic acid-45/45/10-v/v/v followed by a final extraction with acetonitrile /formic acid (FA)-95/05-v/v. Extracted peptides were then analyzed using an Ultimate 3000 nano-RSLC (Thermo Scientific) coupled in line with an Orbitrap ELITE (Thermo Scientific). Peptides were separated on a C18 nano-column with a linear gradient of acetonitrile and analyzed with in a Top 20 collision-induced dissociation data-dependent mass spectrometry with an inclusion list. Data were processed by database searching using SequestHT (Thermo Fisher Scientific) with Proteome Discoverer 1.4 software (Thermo Fisher Scientific) or against a homemade database of all potential three frames translated proteins or peptides from the human NOTCH2NLC 5'UTR sequences. Precursor and fragment mass tolerance were set at 7 ppm and 0.5 Da respectively. Oxidation (M) and Nterminal Acetylation were set as variable modification, and Carbamidomethylation (C) as fixed modification. Peptides were filtered with the Fixed value node of Proteome Discoverer 1.4.

Antibody production

To generate monoclonal antibodies directed against uN2polyG, two months old female BALB/c mice were injected intraperitoneally with KLH conjugated peptides (4D12: CAARPPRMH, 4C4: CSVEMAMNPV) with 200 ug of poly(I/C) as adjuvant. Three injections were performed at 2 weeks intervals and four days prior to hybridoma fusion, mice with positively reacting sera were re-injected. Spleen cells were fused with Sp2/0.Agl4 myeloma cells. Supernatants of hybridoma cultures were tested at day 10 by ELISA for cross-reaction with peptides. Positive supernatants were then tested by Immunofluorescence and western blot on transfected HEK293 cells. Specific cultures were cloned twice on soft agar. Specific hybridomas were established and ascites fluid was prepared by injection of

2x106 hybridoma cells into Freund adjuvant-primed BALB/c mice. All animal experimental procedures were performed according to the French and European authority guidelines.

AAV production and retro-orbital injection

Recombinant AAV2/PHP.eB were generated by tri-transfection of HEK293 cells with pAAV2-GFP, -uN2C-GFP or -uN2CpolyG-GFP with pUCmini-iCAP-PHP.eB and pAD-DELTA-F16. Recombinant vectors were purified by double cesium chloride ultracentrifugation gradients from cell lysates, followed by dialysis and concentration against sterile PBS. Particles were quantified by real time PCR and vector titers were expressed as viral genomes per ml (vg/ml). 2 months old C57BL/6 male mice were injected retro-orbitally with 100 μL of sterile PBS with 1.5x10EXP13 vg/kg of AAV2/PHP.eB.

Animal phenotyping

Rotarod test (Bioseb, Chaville, France) was performed with three testing trials during which the rotation speed accelerated from 4 to 40 rpm in 5 min. Trials were separated by 10-15 min interval. The average latency was used as index of motor coordination performance. Grip test: this test measures the maximal muscle strength (g) using an isometric dynamometer connected to a grid (Bioseb). Mice were allowed to grip the grid with all its paws then they were pulled backward until they released it. Each mouse was submitted to 3 consecutive trials. The maximal strength developed by the mouse before releasing the grid was recorded and the average value of the three trials adjusted to body weight. Notched bar test: mice were tested under 100-lux lighting on a 2 cm-wide and 50 cm-long natural wooden piece notched bar comprising 12 platforms of 2 cm spaced by 13 gaps of 2 cm and bearing a 6 cm^2 terminal platform. Animals had to cross the notched bar twice for training and 3 times for the test. Every instance of a back paw going through the gap was considered an error, and the global error percentage was calculated. Open field test: mice were tested in automated open fields (Panlab, Barcelona, Spain), each virtually divided into central and peripheral regions. The open fields were placed in a room homogeneously illuminated at 120 Lux. Each mouse was placed in the periphery of the open field and allowed to explore freely the apparatus for 30 min, with the experimenter out of the animal's sight. The distance traveled, the number of rears, and time spent in the central and peripheral regions were recorded over the test session. The number of entries and the percent time spent in center area are used as index of emotionality/anxiety

X-ray and UVA-laser irradiation

U2OS cells expressing uN2C with 12 or 100 glycine GFP-tagged were X-ray irradiated for 10 minutes at 10 Gy in a CellRad (Precision). UV-laser micro-irradiation of U2OS cells expressing GFP-tagged U2C with 12 or 100 glycine seeded onto glass-bottom dishes was performed with a spinning disk Yokogawa X1 equipped with a Nikon microscope. For scanning irradiation, we use UV laser 266 nm pulse width < 1 ns power 15 mW and one repetition for each irradiation area. For GFP signal, we use time-lapse spinning disk acquisition with 491 nm 100 mW diode laser, the complete system is customized by Gataga System (Massy-France) and controlled with Metamorph Software.

Immunofluoresence and immunchemistry

For immunofluorescence, mouse or human brain sections were deparaffinized for 10 min in Histosol Plus (LifeScienceProducts) and dehydrated as follows: ethanol 100% (10 min), ethanol 90% (5 min), ethanol 70% (5 min), and rinsed in water. Antigen retrieval was performed in pressure cooker in 10 mM Tris PH9, 1 mM EDTA followed by blocking 1 h with PBS, 0,5% Triton X-100 and 5% Horse Serum. Glass coverslips containing plated cells or brain sections treated as described above were fixed for 15 min in PBS with 4% paraformaldehyde, washed with PBS and incubated in PBS plus 0.5% Triton X-100 during 10 min. The cells were washed three times with PBS and the coverslips were incubated during one hour with primary antibody against Calbindin (Abcam ab82812, 1/200), γH2AX (Abcam ab81299, 1/300), ubiquitin (Abcam ab134953, 1/100), Sumo2/3 (Abcam ab3742, 1/100), p62/Sqstm1 (Abcam ab109012, 1/1000), GFAP (Proteintech 16825-1-AP, 1/250), MAP2 (Abcam ab7756, 1/200) and uN2C 4C4 or 4D12 (mouse monoclonal homemade, 1/100). After washing with PBS, the coverslips were incubated with goat anti mouse secondary antibody conjugated with Alexa 488 or CY3 (Interchim SA) for one hour, washed twice with PBS and incubated for 3 min in PBS/DAPI (1/10 000 dilution). Coverslips were rinsed twice before mounting in Pro-Long media (Molecular Probes) and were examined using a Leica microscope. For immunochemistry, mouse brain sections were deparaffinized 10 min in Histosol Plus (LifeScienceProducts) and dehydrated as follows: ethanol 100% (10 min), ethanol 90% (5 min), ethanol 70% (5 min), and rinsed in water. Antigen retrieval was performed in pressure cooker in 10 mM Tris PH9, 1 mM EDTA followed with 10 μg/ml protein kinase treatment for 20 min at 37°c. Endogenous peroxidase activity was blocked, and blocking 1 h with PBS, 0,5% Triton X-100 and 5% Horse Serum and immunostaining was performed overnight at 4°C using antibody against Calbindin (Abcam ab82812, 1/50), Gfap (Proteintech, 16825-1-AP, 1/100), Sumo2/3 (Abcam ab3742, 1/100) and uN2C 4C4 or 4D12 (mouse monoclonal homemade, 1/100). Antigen–antibody complexes were visualized by incubation with DAB substrate (Abcam) and slides were counterstained with hematoxylin and eosin.

Lysostaphin treatment

HEK293 cells transfected with a uN2CpolyGFP construct were scrapped in PBS 1X and centrifuged during 10 min at 3000 rpm at 4°C. The cell pellet was resuspended in 400 μl of RIPA and 16 μl of cell extract was incubated with 1 μg of lysostaphin (Prospec, ENZ-269) during 5 to 15 minutes at 37°C. Laemmli buffer was add to the mix and proteins were analyze by western blot.

Co-immunoprecipitation assay

24 h after transfection of HEK293 cells with 1 μg of uN2C-GFP constructs in Lipofectamine 2000 (Invitrogen), cells were lysed in RIPA buffer (50 mM Tris-HCl pH 7.5, 0.15 M NaCl, 0.5% Triton X-100) supplemented with protease inhibitor cocktail (Roche) and clarified by centrifugation at 14000 rpm for 10 min. Immunoprecipitations were performed at 4°C for 1 h using pre-washed Anti-GFP (Abcam ab193983) or anti-HA (Pierce 88837) Magnetic Beads in RIPA buffer, washed three time, then bound proteins were eluted by 3 min denaturation step at 95°C with Laemmli buffer followed by mass spectrometry or western blot.

Western blotting

Proteins were denatured 3 min at 95°C, separated on 4%–12% bis-Tris Gel (NuPAGE), transferred on nitrocellulose membranes (Whatman Protan), blocked with 5% non-fat dry milk in Tris Buffer Saline buffer (TBS), incubated with anti-GFP (Abcam ab290), HA (Abcam ab130275), FLAG (Thermofisher PA1-984B), γH2AX (Abcam ab81299), H2AX (Abcam ab229914), Ku70 (SantaCruz sc-56129), Ku80 (Abcam ab 119935), GAPDH (Abcam ab125247) in TBS plus 5% non-fat dry milk, washed 3 times and incubated with anti-rabbit or mouse Peroxidase antibody (1:10,000, Cell Signaling) 1 hour in TBS, followed by washing and ECL Prime chemiluminescence revelation kit (Sigma).

Quantitative real time RT-PCR

Total RNAs from mouse tissues or cells were isolated by TriReagent (Merck). cDNAs were generated using the Transcriptor High Fidelity cDNA synthesis kit (Sigma) for quantification of mRNAs. qPCR were realized using the LightCycler 480 SYBR Green I Master (Roche) in a Lightcycler 480 (Roche) with 15 min at 94°C followed by 50 cycles of 15 s at 94°C, 20 s at 58°C and 20 s at 72°C. *RPLPO* mRNA was used as standard and data were analyzed using the Lightcycler 480 analysis software (2ΔCt method).

QUANTIFICATION AND STATISTICAL ANALYSIS

To eliminate bias, image or animal analyzes were either completely automated or blinded. All statistical analyses were performed using Excel (Microsoft) and Prism (GraphPad). Experiments are represented as either mean value ± Standard Error of Mean (SEM) or box-and-whisker plots with box upper and lower limits representing the 25th and 75th quartiles, respectively, the whiskers depicting the lowest and highest data points and the horizontal line through the box represent the median. The statistical tests used are two-tailed paired Student's t test or ANOVA. Significance was set as $*p < 0.05$; $**p < 0.005$ and $***p < 0.001$. Sample-sizes were determined based on past experiments and to minimize the number of mice used. No statistical method was used to determine whether data meet assumptions of the statistical approach. Detailed statistical information, including the statistical test, measures, number "n" of animals, cells and/ or experiments are indicated in the figures and their respective legends.

Neuron, Volume *109*

Supplemental information

Translation of GGC repeat expansions into a toxic polyglycine protein in NIID defines a novel class of human genetic disorders: The polyG diseases

Manon Boivin, Jianwen Deng, Véronique Pfister, Erwan Grandgirard, Mustapha Oulad-Abdelghani, Bastien Morlet, Frank Ruffenach, Luc Negroni, Pascale Koebel, Hugues Jacob, Fabrice Riet, Anke A. Dijkstra, Kathryn McFadden, Wiley A. Clayton, Daojun Hong, Hiroaki Miyahara, Yasushi Iwasaki, Jun Sone, Zhaoxia Wang, and Nicolas Charlet-Berguerand

Supplemental Information

Translation of GGC repeat expansions into a toxic polyglycine protein in NIID defines a novel class of human genetic disorders: the polyG diseases.

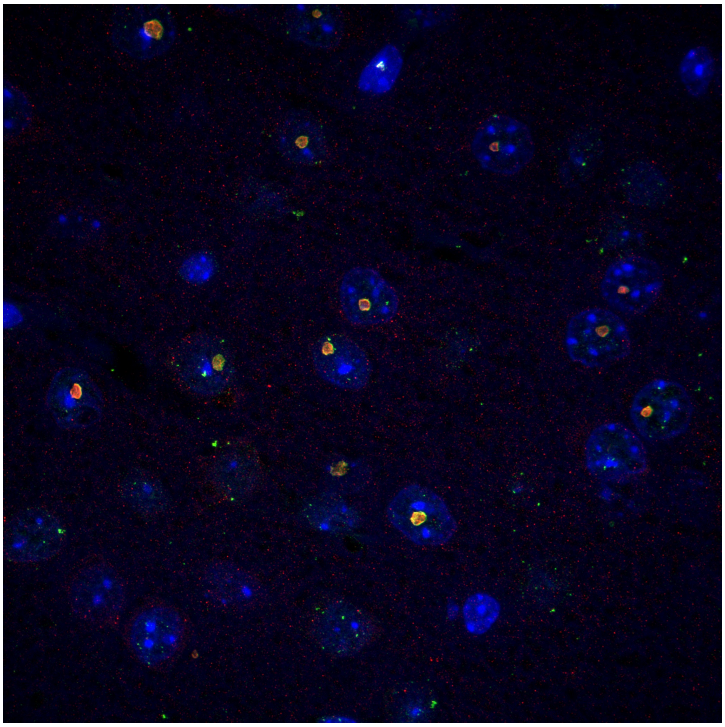

P62 (green) and uN2CpolyG (red)
staining in cortical area of NIID mouse model

A

NOTCH2NLC (N2C) exon1 (GGC)100x *BamHI* GFP (+1 frame, glycine frame):

GCTGAGGCGGCGGCCGAGGAGCGGCGGACTCGGGGCGCGGGGAGTCGAGGCATTTGCGCCTGTGCTTCGGACCGTAGCGCCAGGGCCTGAGCCTTTGAAGCAGGAGGAG
GGGAGGAGAGAGTGGGGCTCCTCTATCGGGACCCCCTCCCC**ATG**TGGATCTGCCCA**GGCGGCGGC…GGCGGCGGC**GACCGAGAAGATGCCCGCCCTGCGCCGCTCTGCT
GTGGGCGCTGCTGGCGCTCTGGCTGTGCTGCGCGACCCCCGCGCATGggatccGTCAGCAAAGGCGAGGAGCTTTTCACCGGGGTTGTTCCCATCCTCGTCGAGCTCGACGGC
GACGTAAACGGCCACAAATTCAGCGTTTCCGGCGAGGGCGAGGGCGATGCCACCTACGGCAAGCTCACCCTCAAGTTCATCTGCACCACCGGCAAGCTCCCCGTCCCCTGGC
CCACCCTCGTCACCACCCTCACCTACGGCGTCCAGTGCTTCAGCCGCTACCCCGACCACATGAAGCAGCACGACTTCTTCAAGTCCGCCATGCCCGAAGGCTACGTCCAGGA
GCGCACCATCTTCTTCAAGGACGACGGCAACTACAAGACCCGCGCCGAGGTGAAGTTCGAGGGCGACACCCTGGTGAACCGCATCGAGCTGAAGGGCATCGACTTCAAGGAG
GACGGCAACATCCTGGGGCACAAGCTGGAGTACAACTACAACAGCCACAACGTCTATATCATGGCCGACAAGCAGAAGAACGGCATCAAGGTGAACTTCAAGATCCGCCACAA
CATCGAGGACGGCAGCGTGCAGCTCGCCGACCACTACCAGCAGAACACCCCCATCGGCGACGGCCCCGTGCTGCTGCCCGACAACCACTACCTGAGCACCCAGTCCGCCCT
GAGCAAAGACCCCAACGAGAAGCGCGATCACATGGTCCTGCTGGAGTTCGTGACCGCCGCCGGGATCACTCTCGGCATGGACGAGCTGTACAAGTAG

B

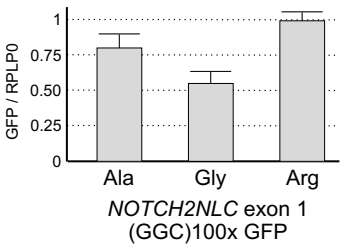

C

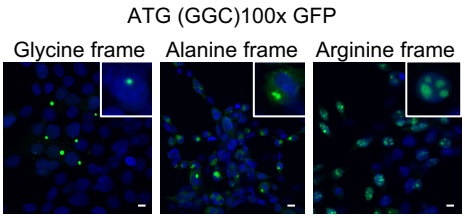

D

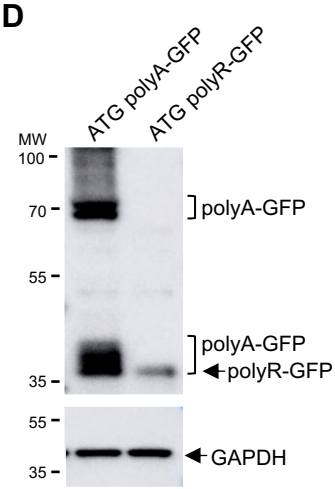

E

Ion Series | Neutral Losses | Precursor Ions

#1	a+	a2+	b+	b2+	Seq.	y+	y2+	#2
1	146.06341	73.53534	174.05833	87.53280	M-Acetyl			20
2	332.14272	166.57500	360.13764	180.57246	W	1587.67171	794.33949	19
3	445.22679	223.11703	473.22170	237.11449	I	1401.59240	701.29984	18
4	605.25744	303.13236	633.25235	317.12981	C-Carbami...	1288.50834	644.75781	17
5	702.31020	351.65874	730.30512	365.65620	P	1128.47769	564.74248	16
6	759.33166	380.16947	787.32658	394.16693	G	1031.42492	516.21610	15
7	816.35313	408.68020	844.34804	422.67766	G	974.40346	487.70537	14
8	873.37459	437.19093	901.36951	451.18839	G	917.38200	459.19464	13
9	930.39606	465.70167	958.39097	479.69912	G	860.36053	430.68390	12
10	987.41752	494.21240	1015.41243	508.20986	G	803.33907	402.17317	11
11	1044.43898	522.72313	1072.43390	536.72059	G	746.31760	373.66244	10
12	1101.46045	551.23386	1129.45536	565.23132	G	689.29614	345.15171	9
13	1158.48191	579.74459	1186.47682	593.74205	G	632.27468	316.64098	8
14	1215.50337	608.25533	1243.49829	622.25278	G	575.25321	288.13025	7
15	1272.52484	636.76606	1300.51975	650.76351	G	518.23175	259.61951	6
16	1329.54630	665.27679	1357.54122	679.27425	G	461.21029	231.10878	5
17	1386.56776	693.78752	1414.56268	707.78498	G	404.18882	202.59805	4
18	1443.58923	722.29825	1471.58414	736.29571	G	347.16736	174.08732	3
19	1558.61617	779.81172	1586.61109	793.80918	D	290.14590	145.57659	2
20					R	175.11895	88.06311	1

M^{Ac}WICPGGGGGGGGGGGGGDR

F

NOTCH2NLC (N2C) exons 1 to 2:

CCAAACTTCGGGCGGCGGCTGAGGCGGCGGCCGAGGAGCGGCGGACTCGGGGCGCGGGGAGTCGAGGCATTTGCGCCTGT
GCTTCGGACCGTAGCGCCAGGGCCTGAGCCTTTGAAGCAGGAGGAGGGGAGGAGAGAGTGGGGCTCCTCTATCGGGACCCC
CTCCCC**ATG**TGGATCTGCCCA**GGCGGCGGC…GGCGGCGGC**GGAGGAGGCGGCGACCGAGAAGATGCCCGCCCTGCGCCG
CTCTGCTGTGGGCGCTGCTGGCGCTCTGGCTGTGCTGCGCGACCCCCGCGCATGgtgagta…intron1…atttttagCATTGCAGTGTC
GAGATGGCTATGAACCCTGTG**TAA**ATGAAGGA**ATG**TGTGTTACCTACCACAATGGCACAGGATACTGCAAgtaagttt…intron2

ATG N2C

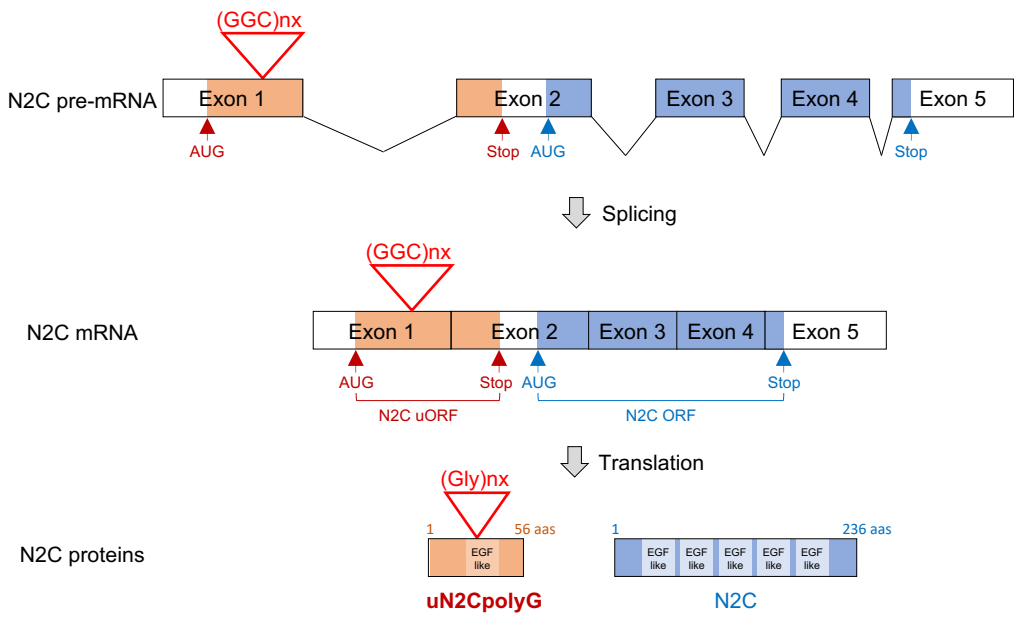

Figure S1. Related to Figure 1.

Figure S1. Related to Figure 1.
***NOTCH2NLC* GGC repeats are translated into polyglycine.**

(**A**) Sequence of the human *NOTCH2NLC* exon 1 with GGC repeats fused to the GFP in the glycine frame and cloned into pcDNA3.

(**B**) RT-qPCR of the GFP and *RPLP0* mRNA expression of HEK293 cells transfected for 24 hours with GGC repeats embedded in the *NOTCH2NLC* exon 1 and fused to the GFP in either the glycine, alanine or arginine frame.

(**C**) GFP fluorescence of HEK293 cells transfected for 24 hours with 100 GGC repeats cloned downstream of an artificial ATG start codon and fused to the GFP in the three possible frames.

(**D**) Immunoblot against the GFP or the GAPDH of HEK293 cells transfected for 24 hours with 100 GGC repeats cloned downstream of an artificial ATG start codon and fused to the GFP in either the alanine or the arginine frame, encoding either a polyalanine or a polyarginine-containing protein, respectively.

(**E**) LC-MS/MS table analysis of the N-terminal peptide from GFP-immunoprecipitated and trypsin digested protein expressed from HEK293 cells transfected with *NOTCH2NLC* exon 1 with GGC repeats and fused to the GFP in the glycine frame.

(**F**) Upper panel, sequence of the human *NOTCH2NLC* exons 1 to 2. Exon sequences are in upper cases, intronic sequences are in grey lower cases. Lower panel, scheme of the *NOTCH2NLC* transcript encoding the upstream (uN2C) and main (N2C) ORFs, which contain 1 and 5 potential EGF-like domains, respectively. Upstream (uN2C) and main (N2C) NOTCH2NLC ORFs are indicated in orange and blue, respectively.

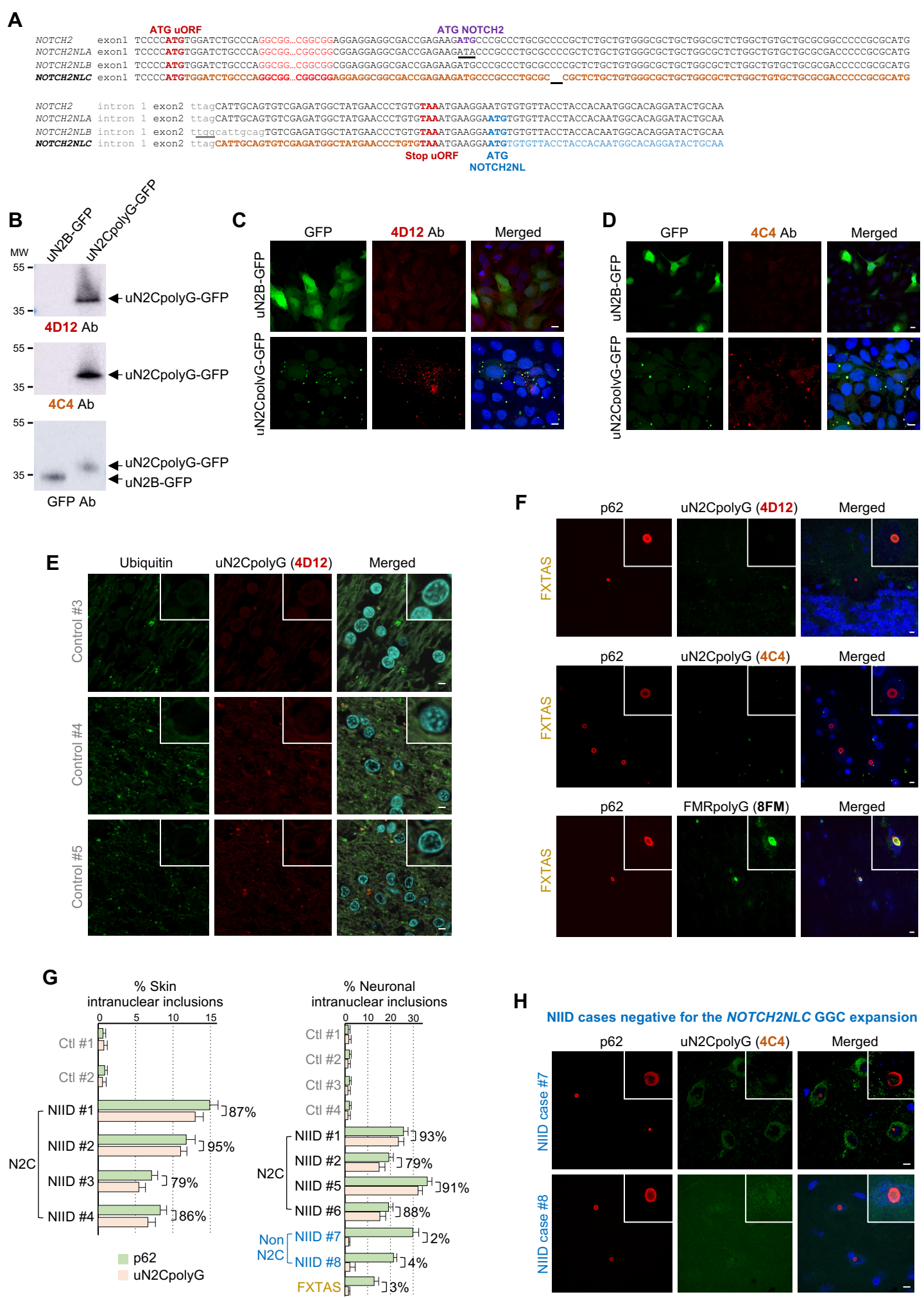

Figure S2. Related to Figure 2.

Figure S2. Related to Figure 2.
uN2polyG is present in NIID nuclear inclusions.

(**A**) Alignment of *NOTCH2* and *NOTCH2NLA*, B and C exons 1 and 2 sequences. Exon sequences are in upper cases, intronic sequences are in grey lower cases. Sequence encoding the *NOTCH2NLC* upstream (uN2C) and main (N2C) ORFs are indicated in orange and blue, respectively. ATG start and stop codons of the potential upstream ORFS are indicated in bold red, while ATG start codons of the NOTCH2NL main ORFs are indicated in bold blue. Of interest, NOTCH2NL proteins are likely cytosolic, as they start in exon 2 and thus lack NOTCH2 peptide signal sequence encoded by the exon 1. Absence of peptide signal in NOTCH2NL proteins is caused by different mechanisms, as the corresponding *NOTCH2* ATG start codon in exon 1 is absent in *NOTCH2NLA* and out of frame in *NOTCH2NLB* and *NOTCH2NLC* due to either mutation of the 3' splice site of *NOTCH2NLB* intron 1 or deletion of 2 nucleotides in *NOTCH2NLC* exon 1. Mutations of *NOTCH2NLA* ATG and *NOTCH2NLB* 3' splice site as well as the 2-nts deletion within *NOTCH2NLC* exon 1 are underlined.

(**B**) Immunoblot of uN2B-GFP or uN2CpolyG-GFP transfected HEK293 cells with 4C4, 4D12 and anti-GFP antibodies.

(**C**, **D**) GFP fluorescence and immunofluorescence of uN2B-GFP and uN2CpolyG-GFP transfected HEK293 cells using either 4D12 (**C**) or 4C4 (**D**) antibody.

(**E**) Control immunofluorescence against uN2CpolyG (4D12 antibody) and ubiquitin on brain sections of control individuals.

(**F**) Immunofluorescence against p62 and either uN2CpolyG (4D12 or 4C4 antibody) or FMRpolyG (8FM antibody) on brain sections of a FXTAS case, carrier of an expansion of CGG repeats within the 5'UTR of the *FMR1* gene.

(**G**) Quantification of p62 or uN2CpolyG-positive intranuclear inclusions per 100 nuclei in skin (left panel) or brain (right panel) sections of control, FXTAS or NIID (carrier or not of an expansion of GGC repeats within *NOTCH2NLC*) individuals. Brackets indicate the percentage of co-localization between p62- and uN2polyG-positive intranuclear inclusions. At least 100 nuclei were counted per individual.

(**H**) Immunofluorescence against p62 and uN2CpolyG (4C4 antibody) on brain sections of two European NIID cases negative for the *NOTCH2NLC* GGC mutation.

Scale bars, 10 µm. Nuclei were counterstained with DAPI.

A

uN2C HA :
MWICP **(G)12x or 100x** DREDARPAPLCCGRCWRSGCAARPPRMHCSVEMAMNPV GSLYPYDVPDYAA.

uN2C GFP :
MWICP **(G)12x or 100x** DREDARPAPLCCGRCWRSGCAARPPRMHCSVEMAMNPV GSVSKGEELFTGVVPILVELDGDVNGHKFSVSGEGEGDATYGKLTLKFICTTGKLPVPW
PTLVTTLTYGVQCFSRYPDHMKQHDFFKSAMPEGYVQERTIFFKDDGNYKTRAEVKFEGDTLVNRIELKGIDFKEDGNILGHKLEYNYNSHNVYIMADKQKNGIKVNFKIRHNIEDGS
VQLADHYQQNTPIGDGPVLLPDNHYLSTQSALSKDPNEKRDHMVLLEFVTAAGITLGMDELYK.

B

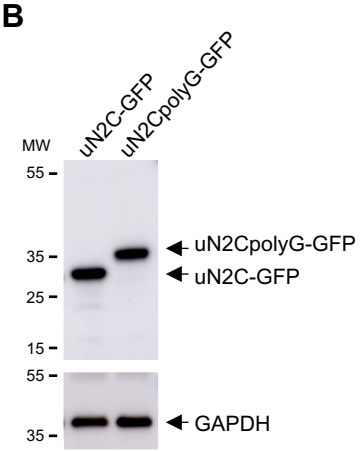

C

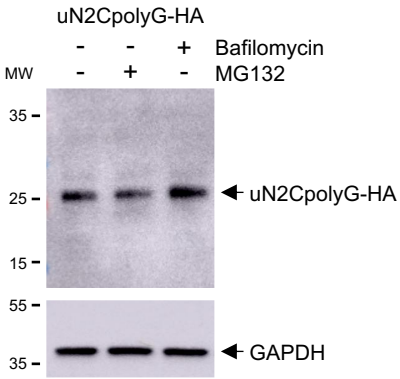

D

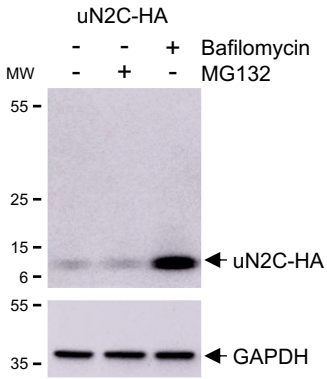

E

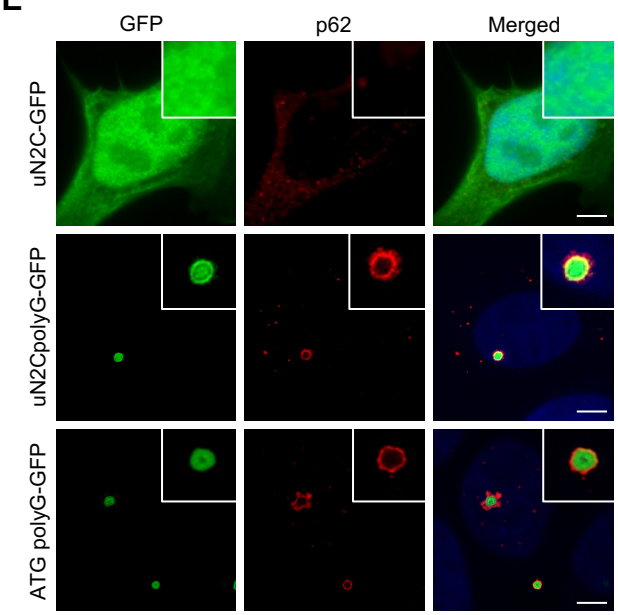

F

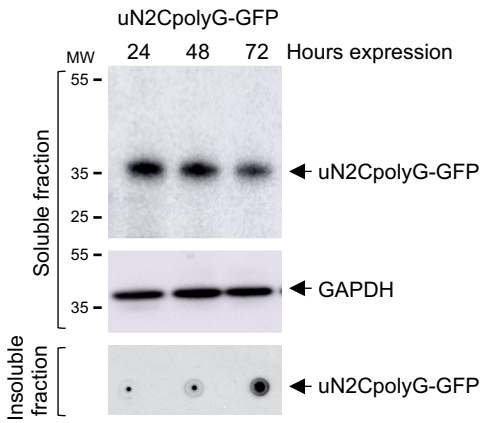

G

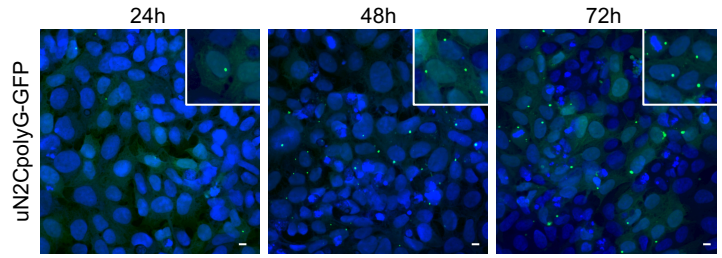

H

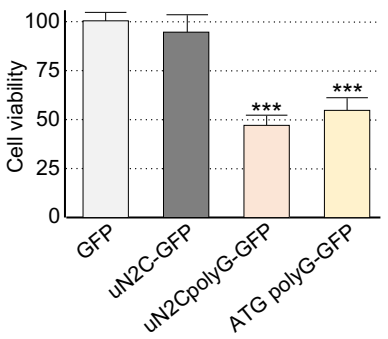

Figure S3. Related to Figure 3.

Figure S3. Related to Figure 3.
Expression of uN2CpolyG is toxic in cell culture.

(**A**) Sequences of the uN2C and uN2CpolyG-HA or -GFP tagged proteins.

(**B**) Immunoblot against the GFP or the GAPDH of proteins extracted from HEK293 cells transfected for 24 hours with uN2C-GFP or uN2CpolyG-GFP.

(**C, D**) Immunoblot against the HA tag or the GAPDH of proteins extracted from HEK293 cells transfected for 24 hours with either uN2CpolyG-HA (C) or uN2C-HA (D) and treated with or without MG132 and/or Bafilomycin A1 for 15 hours.

(**E**) GFP fluorescence and immunofluorescence against p62 of U2OS cells transfected with constructs expressing either the GFP, uN2C-GFP, uN2CpolyG-GFP or ATG polyG-GFP. Scale bars, 5 μm. Nuclei were counterstained with DAPI.

(**F**) Immunoblot on whole cell extract (soluble fraction) or dot blot on urea-treated pellet (insoluble fraction) against the GFP of HEK293 cells transfected with uN2CpolyG-GFP for 24, 48 and 72 hours.

(**G**) GFP fluorescence of U2OS cells expressing uN2CpolyG-GFP for 24, 48 and 72 hours. Scale bars, 10 μm. Nuclei were counterstained with DAPI.

(**H**) Cell viability of GT1-7 neuronal cells transfected for 24 hours with either the GFP, uN2C-GFP, uN2CpolyG-GFP or ATG polyG-GFP. Error bars indicate SEM. Student t-test, *** indicates $p<0.001$.

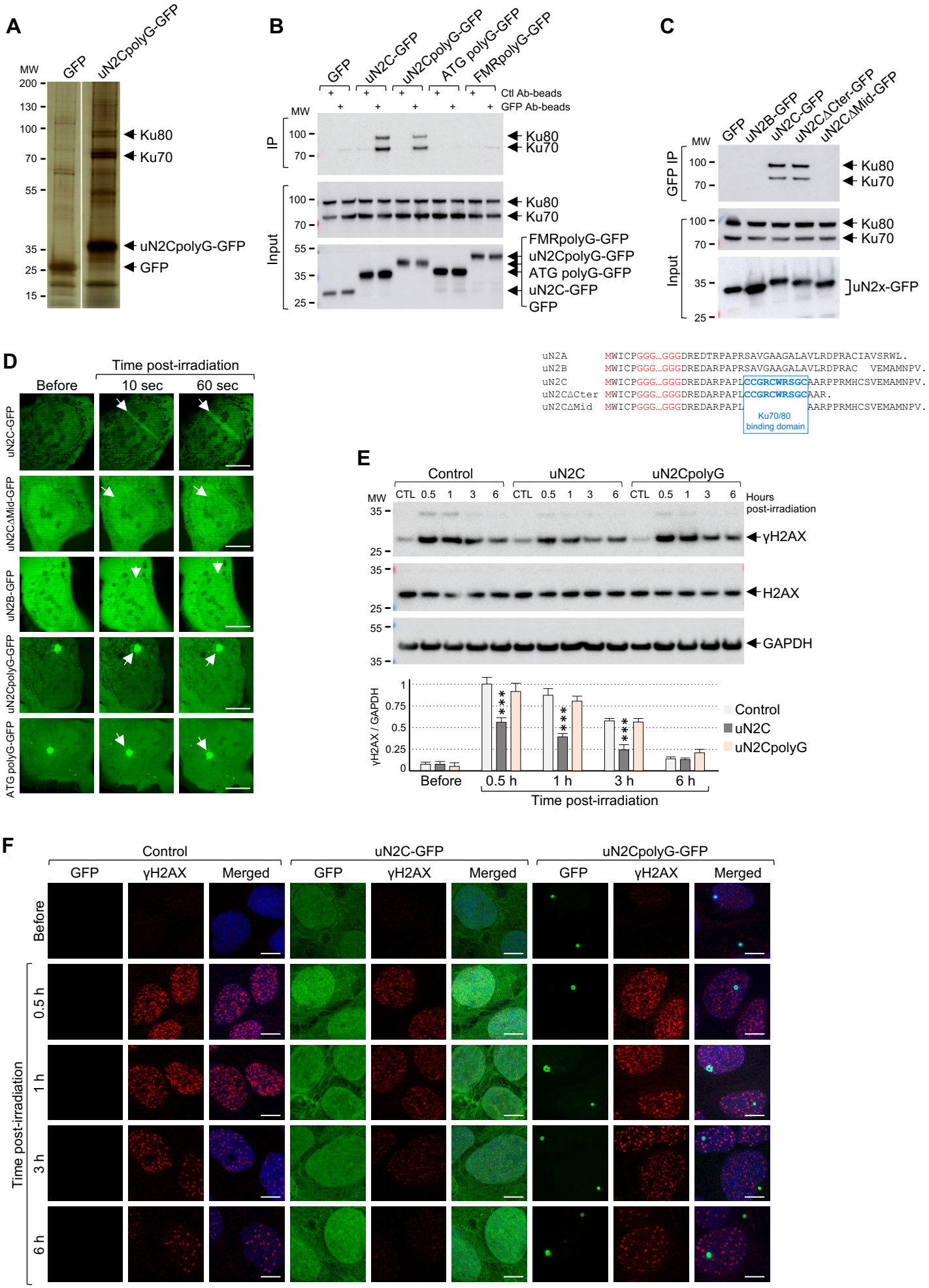

Figure S4. Related to Figure 3.

Figure S4. Related to Figure 3.
The uN2C control protein promotes DNA repair

(**A**) Silver staining of the proteins captured by GFP immunoprecipitation from HEK293 cells transfected for 24 hours with either GFP or uN2CpolyG-GFP.

(**B**) Immunoblot against endogenous Ku70 and Ku80 of either control antibody (anti-HA) or GFP immunoprecipitated proteins (IP) or whole cell lysate (Input) from HEK293 cells transfected for 24 hours with either GFP, uN2C-GFP, uN2CpolyG-GFP, ATG polyG-GFP or FMRpolyG-GFP.

(**C**) Upper panel, immunoblot against endogenous Ku70 and Ku80 of GFP immunoprecipitated proteins or whole cell lysate from HEK293 cells transfected for 24 hours with either GFP, uN2B-GFP or mutants of uN2C-GFP. Lower panel, sequence alignment of the upstream ORFs of *NOTCH2NLA*, *B* and C wild type or mutant constructs. The uN2C amino acid sequence important for binding to Ku proteins is indicated in bold blue.

(**D**) U2OS cells transfected 24 hours with either uN2C-GFP, mutant uN2CΔMid-GFP, uN2B-GFP, uN2CpolyG-GFP or ATG polyG-GFP were subjected to laser micro-irradiation. White arrows indicate laser stripes. Scale bars, 10 μm. Nuclei were counterstained with DAPI.

(**E, F**) Immunoblot against H2AX, γH2AX or the GAPDH (E) or GFP fluorescence and immunofluorescence against γH2AX (F) of control cells or U2OS stably expressing either uN2C-GFP or uN2CpolyG-GFP, X-ray irradiated for 10 minutes, and let to recover for 30 minutes, 1, 3 or 6 hours. Lower panel, quantification of γH2AX / GAPDH ratio before and after X-ray irradiation. Error bars indicate SEM. Student t-test, *** indicates $p<0.001$. Scale bars, 10 μm. Nuclei were counterstained with DAPI.

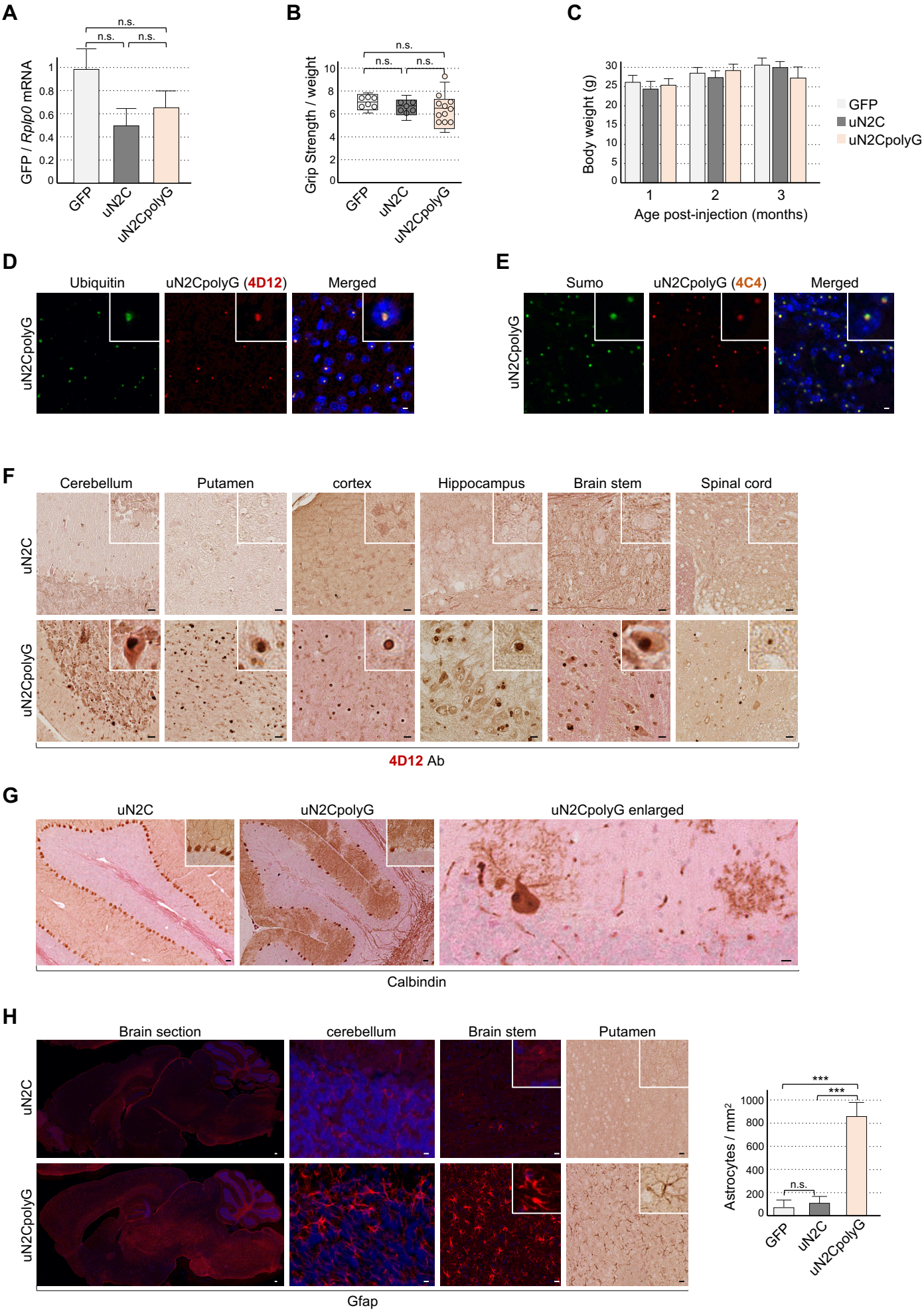

Figure S5. Related to Figure 4.

Figure S5. Related to Figure 4.
Expression of uN2CpolyG is pathogenic in animal.

(**A**) RT-qPCR analysis of GFP expression relative to *Rplp0* mRNA in brain of AAV2/PHP.eB GFP (n=3), uN2C-GFP (n=3) or uN2CpolyG-GFP (n=3) injected mice.

(**B**) Grip test. Maximal force relative to mouse body weight exerted to releases AAV2/PHP.eB GFP (n=6), uN2C-GFP (n=6) and uN2CpolyG-GFP (n=11) injected male mice holding a grid with their forepaws and tested 3 months post-injection. Box-and-whisker plot, box upper and lower limits represent 25th and 75th percentiles, whiskers represent minimum and maximum values and the horizontal line across the box represents the median.

(**C**) Body weight at 1, 2 and 3 months post-injection of AAV2/PHP.eB GFP (n=6), uN2C-GFP (n=6) and uN2CpolyG-GFP (n=11) injected male mice.

(**D**, **E**) Immunofluorescence against uN2CpolyG using either the 4D12 (D) or 4C4 (E) antibody and ubiquitin (D) or sumo (E) on putamen areas of uN2CpolyG-GFP expressing mice scarified 2 months after AAV injection. Scale bars, 10 µm. Nuclei were counterstained with DAPI.

(**F**) Immunohistochemistry against uN2CpolyG of cerebellum, putamen, cortical, hippocampal, brain stem and spinal cord areas of uN2C-GFP and uN2CpolyG-GFP expressing mice scarified 3 months post AAV injection. Sections were counterstained with hematoxylin and eosin. Scale bars, 20 µm.

(**G**) Calbindin immunohistochemistry of cerebellum areas of uN2C-GFP and uN2CpolyG-GFP expressing mice scarified 4 months post AAV injection. Scale bars, 10 µm.

(**H**) Left panel, immunofluorescence or immunohistochemistry against GFAP of brain sections of uN2C-GFP and uN2CpolyG-GFP expressing mice scarified 3.5 months post AAV injection. IF, nuclei were counterstained with DAPI. IHC, sections were counterstained with hematoxylin and eosin. Scale bars, 10 µm. Right panel, quantification of Gfap-positive cells in the putamen of GFP (n=4), uN2C-GFP (n=4) or uN2CpolyG-GFP (n=4) expressing mice. Bar graphs indicate standard error of the mean (SEM). Student t-test, *** indicates $p<0.001$.

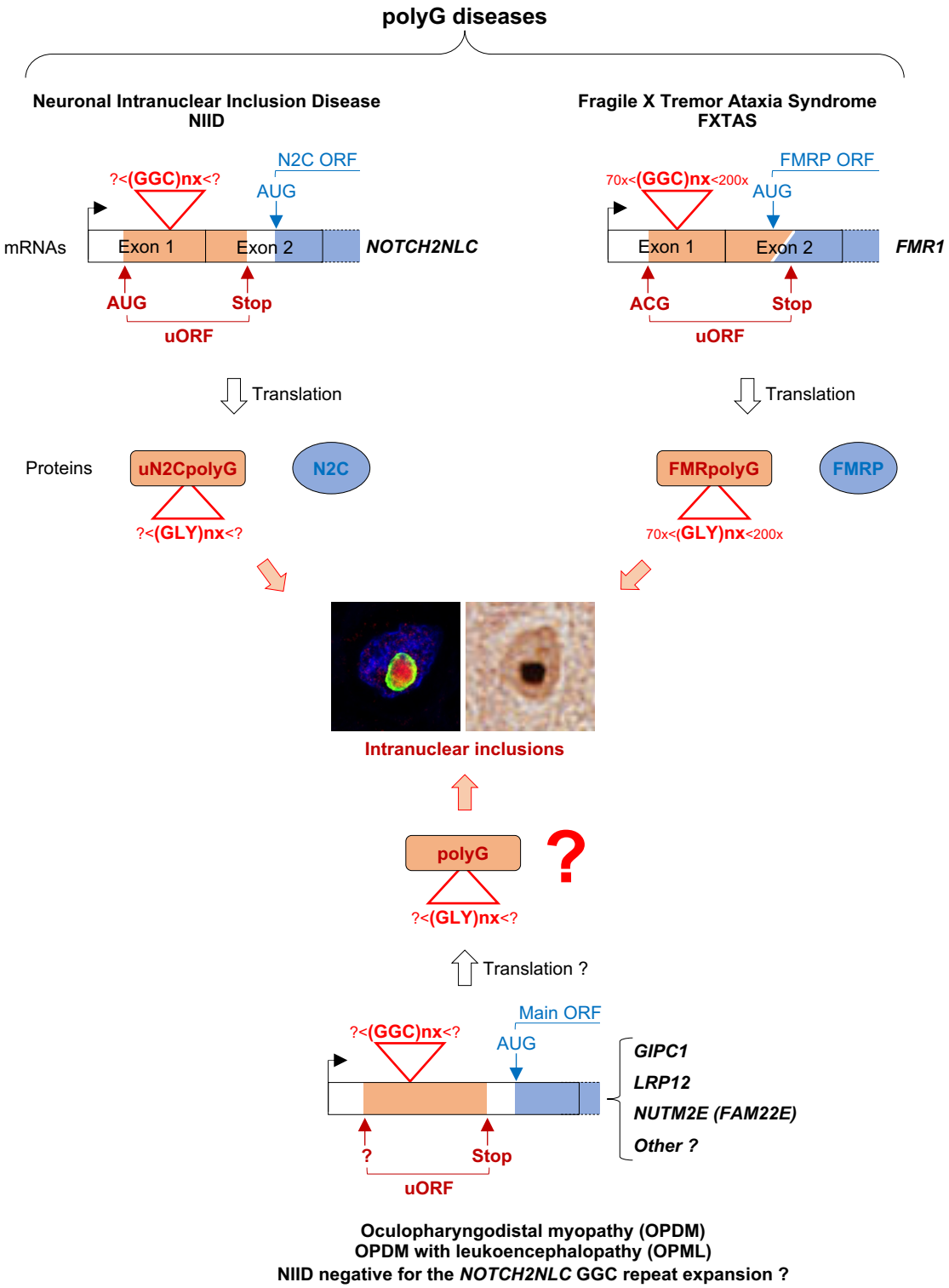

Figure S6. Related to Figure 4.
Model of polyG diseases.

Expanded GGC repeats embedded within upstream ORFs located into *FMR1* and *NOTCH2NLC* 5'UTR are translated into polyglycine containing proteins, FMRpolyG and uN2CpolyG, which are toxic and form p62-positive intranuclear inclusions in FXTAS and NIID, respectively. A similar GGC repeat translation mechanism into yet to discover polyglycine proteins may occur in OPDM and OPML.

Patient	Gender	Age at onset	Duration (months)	Family history	Initial symptom	GGC repeats,	Reference
NIID #1	Female	68	<1	Sporadic	Dizziness & vomiting	102 *NOTCH2NLC*	-
NIID #2	Male	60	12	Sporadic	Paroxysmal encephalopathy	142 *NOTCH2NLC*	Deng et al., 2019
NIID #3	Female	62	60	Familial	Tremor	n.a.	-
NIID #4	Male	63	24	Sporadic	Urinary incontinence	115 *NOTCH2NLC*	-
NIID #5	Male	7	72	Sporadic	Tremor, ataxia,	n.a.	McFadden et al., 2005
NIID #6	Male	30	37	Familial	Muscle weakness	162 *NOTCH2NLC*	Sone et al., 2019
NIID #7	Female	65	3	Sporadic	Memory problems	No expansions *FMR1, NOTCH2NLC*	Cupidi et al., 2019
NIID #8	Male	50	16	Sporadic	Behavioral changes	No expansions *FMR1, NOTCH2NLC*	-
FXTAS	Male	43	22	Familial	Memory problems, aphasia	77 *FMR1*	-
CTL #1	Female	53	-	-	Memory decline	-	-
CTL #2	Female	51	-	-	Urinary difficulties	-	-
CTL #3	Male	66	-	-	Sudden death	-	-
CTL #4	Male	70	-	-	Interstitial pneumonia	-	-
CTL #5	Female	67	-	-	polymyositis	-	-

n.a. Not available

Table S1. Related to Figure 2. Patient information.

Accession	Description	MW [kDa]	Coverage [%]	# Peptides	# PSMs	PSM GFP	PSM uN2CpolyG	uN2cpolyG / GFP
P12956	X-ray repair cross-complementing protein 6 OS=Homo sapiens OX=9606 GN=XRCC6 PE=1 S	70	54	34	460	1	94	94
P13010	X-ray repair cross-complementing protein 5 OS=Homo sapiens OX=9606 GN=XRCC5 PE=1 S	83	76	43	522	1	123	92
P78527	DNA-dependent protein kinase catalytic subunit OS=Homo sapiens OX=9606 GN=PRKDC PE	469	9	24	48	1	36	36
Q16531	DNA damage-binding protein 1 OS=Homo sapiens OX=9606 GN=DDB1 PE=1 SV=1	127	28	23	72	1	41	31
O14744	Protein arginine N-methyltransferase 5 OS=Homo sapiens OX=9606 GN=PRMT5 PE=1 SV=	73	54	26	148	3	32	12
Q9BS26	Endoplasmic reticulum resident protein 44 OS=Homo sapiens OX=9606 GN=ERP44 PE=1 SV	47	48	17	115	3	27	10
P27708	CAD protein OS=Homo sapiens OX=9606 GN=CAD PE=1 SV=3	243	28	42	131	3	26	10
P13639	Elongation factor 2 OS=Homo sapiens OX=9606 GN=EEF2 PE=1 SV=4	95	57	41	211	6	53	9
Q99714	3-hydroxyacyl-CoA dehydrogenase type-2 OS=Homo sapiens OX=9606 GN=HSD17B10 PE=1	27	50	8	39	1	9	9
P61962	DDB1- and CUL4-associated factor 7 OS=Homo sapiens OX=9606 GN=DCAF7 PE=1 SV=1	39	29	8	46	1	12	9
P11586	C-1-tetrahydrofolate synthase, cytoplasmic OS=Homo sapiens OX=9606 GN=MTHFD1 PE=1	102	12	10	34	1	9	9
P30153	Serine/threonine-protein phosphatase 2A 65 kDa regulatory subunit A alpha isoform OS=H	65	42	20	77	2	20	9
P49411	Elongation factor Tu, mitochondrial OS=Homo sapiens OX=9606 GN=TUFM PE=1 SV=2	50	37	13	53	2	14	8
P35579	Myosin-9 OS=Homo sapiens OX=9606 GN=MYH9 PE=1 SV=4	226	12	17	54	1	11	8
Q92945	Far upstream element-binding protein 2 OS=Homo sapiens OX=9606 GN=KHSRP PE=1 SV=	73	37	20	88	2	19	8
Q9H845	Acyl-CoA dehydrogenase family member 9, mitochondrial OS=Homo sapiens OX=9606 GN=	69	16	8	24	1	8	8
Q9BQA1	Methylosome protein 50 OS=Homo sapiens OX=9606 GN=WDR77 PE=1 SV=1	37	33	10	61	2	13	8
P07237	Protein disulfide-isomerase OS=Homo sapiens OX=9606 GN=P4HB PE=1 SV=3	57	23	11	44	1	11	8
P22102	Trifunctional purine biosynthetic protein adenosine-3 OS=Homo sapiens OX=9606 GN=GAR	108	14	9	29	1	8	8
P30048	Thioredoxin-dependent peroxide reductase, mitochondrial OS=Homo sapiens OX=9606 GN	28	51	8	59	2	16	8
O75534	Cold shock domain-containing protein E1 OS=Homo sapiens OX=9606 GN=CSDE1 PE=1 SV=	89	25	15	50	2	13	8
Q9H857	5'-nucleotidase domain-containing protein 2 OS=Homo sapiens OX=9606 GN=NT5DC2 PE=	61	21	10	31	1	10	8
P63151	Serine/threonine-protein phosphatase 2A 55 kDa regulatory subunit B alpha isoform OS=H	52	53	19	74	2	15	7
Q92973	Transportin-1 OS=Homo sapiens OX=9606 GN=TNPO1 PE=1 SV=2	102	13	8	22	1	7	7
P54136	Arginine--tRNA ligase, cytoplasmic OS=Homo sapiens OX=9606 GN=RARS PE=1 SV=2	75	24	11	46	1	10	7
P04843	Dolichyl-diphosphooligosaccharide--protein glycosyltransferase subunit 1 OS=Homo sapien	69	37	15	43	2	14	7
Q13162	Peroxiredoxin-4 OS=Homo sapiens OX=9606 GN=PRDX4 PE=1 SV=1	31	58	13	82	3	19	7
P42771	Cyclin-dependent kinase inhibitor 2A OS=Homo sapiens OX=9606 GN=CDKN2A PE=1 SV=2	17	70	7	33	1	9	7
P31689	DnaJ homolog subfamily A member 1 OS=Homo sapiens OX=9606 GN=DNAJA1 PE=1 SV=2	45	36	9	47	2	12	7
Q5H9R7	Serine/threonine-protein phosphatase 6 regulatory subunit 3 OS=Homo sapiens OX=9606 (	98	28	19	54	2	16	7
P49915	GMP synthase [glutamine-hydrolyzing] OS=Homo sapiens OX=9606 GN=GMPS PE=1 SV=1	77	19	12	29	1	9	7
P63244	Receptor of activated protein C kinase 1 OS=Homo sapiens OX=9606 GN=RACK1 PE=1 SV=	35	50	9	33	1	9	7
Q9Y265	RuvB-like 1 OS=Homo sapiens OX=9606 GN=RUVBL1 PE=1 SV=1	50	28	9	44	1	9	7
P53396	ATP-citrate synthase OS=Homo sapiens OX=9606 GN=ACLY PE=1 SV=3	121	10	8	24	1	7	7
P21333	Filamin-A OS=Homo sapiens OX=9606 GN=FLNA PE=1 SV=4	281	10	17	46	1	9	7
P28482	Mitogen-activated protein kinase 1 OS=Homo sapiens OX=9606 GN=MAPK1 PE=1 SV=3	41	53	15	61	2	13	6
Q93009	Ubiquitin carboxyl-terminal hydrolase 7 OS=Homo sapiens OX=9606 GN=USP7 PE=1 SV=2	128	12	10	25	1	6	6
Q9Y3F4	Serine-threonine kinase receptor-associated protein OS=Homo sapiens OX=9606 GN=STRA	38	46	12	58	2	13	6
O60884	DnaJ homolog subfamily A member 2 OS=Homo sapiens OX=9606 GN=DNAJA2 PE=1 SV=1	46	23	7	23	1	6	6
P67775	Serine/threonine-protein phosphatase 2A catalytic subunit alpha isoform OS=Homo sapien	36	56	12	61	2	15	6
P27361	Mitogen-activated protein kinase 3 OS=Homo sapiens OX=9606 GN=MAPK3 PE=1 SV=4	43	28	8	30	1	8	6
P45880	Voltage-dependent anion-selective channel protein 2 OS=Homo sapiens OX=9606 GN=VDA	32	43	8	31	1	8	6
P22234	Multifunctional protein ADE2 OS=Homo sapiens OX=9606 GN=PAICS PE=1 SV=3	47	40	14	76	3	16	6
P17812	CTP synthase 1 OS=Homo sapiens OX=9606 GN=CTPS1 PE=1 SV=2	67	26	12	48	2	12	6
Q9UK99	F-box only protein 3 OS=Homo sapiens OX=9606 GN=FBXO3 PE=1 SV=3	55	26	10	33	2	10	6
P13489	Ribonuclease inhibitor OS=Homo sapiens OX=9606 GN=RNH1 PE=1 SV=2	50	36	12	43	2	10	6
O00429	Dynamin-1-like protein OS=Homo sapiens OX=9606 GN=DNM1L PE=1 SV=2	82	19	10	24	1	8	6
P29966	Myristoylated alanine-rich C-kinase substrate OS=Homo sapiens OX=9606 GN=MARCKS PE	32	45	9	54	2	10	6
P49327	Fatty acid synthase OS=Homo sapiens OX=9606 GN=FASN PE=1 SV=3	273	32	50	206	8	46	6
P49366	Deoxyhypusine synthase OS=Homo sapiens OX=9606 GN=DHPS PE=1 SV=1	41	47	11	47	3	16	6
O95831	Apoptosis-inducing factor 1, mitochondrial OS=Homo sapiens OX=9606 GN=AIFM1 PE=1 S	67	20	9	27	1	8	6
Q9UQ80	Proliferation-associated protein 2G4 OS=Homo sapiens OX=9606 GN=PA2G4 PE=1 SV=3	44	28	8	35	1	7	6
P42704	Leucine-rich PPR motif-containing protein, mitochondrial OS=Homo sapiens OX=9606 GN=	158	12	14	29	2	9	5
P31939	Bifunctional purine biosynthesis protein PURH OS=Homo sapiens OX=9606 GN=ATIC PE=1	65	19	7	16	1	5	5
Q15654	Thyroid receptor-interacting protein 6 OS=Homo sapiens OX=9606 GN=TRIP6 PE=1 SV=3	50	26	8	16	1	5	5
P22314	Ubiquitin-like modifier-activating enzyme 1 OS=Homo sapiens OX=9606 GN=UBA1 PE=1 S	118	34	25	110	5	24	5
Q13263	Transcription intermediary factor 1-beta OS=Homo sapiens OX=9606 GN=TRIM28 PE=1 SV	89	37	16	86	3	17	5
Q8IXB1	DnaJ homolog subfamily C member 10 OS=Homo sapiens OX=9606 GN=DNAJC10 PE=1 SV=	91	17	11	31	2	10	5
P25205	DNA replication licensing factor MCM3 OS=Homo sapiens OX=9606 GN=MCM3 PE=1 SV=3	91	22	15	57	2	10	5
Q96QK1	Vacuolar protein sorting-associated protein 35 OS=Homo sapiens OX=9606 GN=VPS35 PE=	92	28	18	58	3	13	5
P29590	Protein PML OS=Homo sapiens OX=9606 GN=PML PE=1 SV=3	98	9	7	16	1	5	5
P10599	Thioredoxin OS=Homo sapiens OX=9606 GN=TXN PE=1 SV=3	12	54	6	67	3	14	5
P55060	Exportin-2 OS=Homo sapiens OX=9606 GN=CSE1L PE=1 SV=3	110	8	7	20	1	6	5
Q96J01	THO complex subunit 3 OS=Homo sapiens OX=9606 GN=THOC3 PE=1 SV=1	39	33	8	22	1	6	5
P26639	Threonine--tRNA ligase, cytoplasmic OS=Homo sapiens OX=9606 GN=TARS PE=1 SV=3	83	19	10	30	2	9	5
P05141	ADP/ATP translocase 2 OS=Homo sapiens OX=9606 GN=SLC25A5 PE=1 SV=7	33	29	8	38	2	9	5
P05023	Sodium/potassium-transporting ATPase subunit alpha-1 OS=Homo sapiens OX=9606 GN=	113	16	12	39	2	11	5
Q13185	Chromobox protein homolog 3 OS=Homo sapiens OX=9606 GN=CBX3 PE=1 SV=4	21	29	5	24	1	6	5
P31040	Succinate dehydrogenase [ubiquinone] flavoprotein subunit, mitochondrial OS=Homo sapie	73	31	12	42	3	12	5

Table S2. Related to Figure 3. Proteins interacting with uN2CpolyG.
Mass spectrometry analysis of GFP-trap immunoprecipitated proteins from HEK293 cells expressing either the GFP or uN2CpolyG-GFP.